



ELSEVIER

Contents lists available at ScienceDirect

International Journal of Disaster Risk Reduction

journal homepage: www.elsevier.com/locate/ijdrr

UAV and GIS based rapid earthquake-induced building damage assessment and methodology for EMS-98 isoseismal map drawing: The June 12, 2017 Mw 6.3 Lesvos (Northeastern Aegean, Greece) earthquake

Spyridon Mavroulis^{a,*}, Emmanouil Andreadakis^a, Nafsika-Ioanna Spyrou^a, Varvara Antoniou^a, Emmanouel Skourtsos^a, Panayotis Papadimitriou^b, Ioannis Kassaras^b, George Kaviris^b, Gerasimos - Akis Tselentis^b, Nikolaos Voulgaris^b, Panayotis Carydis^c, Efthymios Lekkas^a

^a Department of Dynamic Tectonic Applied Geology, Faculty of Geology and Geoenvironment, School of Sciences, National and Kapodistrian University of Athens, Greece

^b Department of Geophysics and Geothermy, Faculty of Geology and Geoenvironment, School of Sciences, National and Kapodistrian University of Athens, Greece

^c National Technical University of Athens, Greece

ARTICLE INFO

Keywords:

Building damage
EMS-98
UAV
Web GIS
Lesvos
Greece

ABSTRACT

On June 12, 2017, an Mw 6.3 earthquake struck Lesvos Island (Northeastern Aegean, Greece). Building damage was observed in its southeastern part with very heavy structural damage limited in the settlement of Vrissa. Taking into account that Vrissa is located further inland from the epicenter than other settlements with less damage, Vrissa looks like an earthquake impact paradox. For interpreting this paradox, a complete approach for damage assessment in an earthquake-affected area was applied during the first hours of the emergency response phase in order to provide crucial information to civil protection agencies. It comprises integration of building-by-building inspection, use of desktop and web GIS applications, UAV survey and digital post processing, extraction of data and information related to the buildings of the affected area, application of the European Macroseismic Scale 1998 and assignment of macroseismic intensities. Correlation of the all aforementioned data with the geological, geomorphological, geotechnical and seismological properties of the affected area along with its buildings characteristics was followed. This damage scene is attributed to the synergy of the near-field location of Vrissa, recent deposits, geotechnically unstable zones, proximity to active faults, rupture directivity phenomena and vulnerable buildings. The integration of UAV and web GIS applications during a rapid post-earthquake field macroseismic reconnaissance can potentially be considered as a methodological framework that can be applied for similar analysis in other areas affected not only by earthquakes but also by other extreme events that have the potential to cause destructive effects on the natural environment, humans and infrastructures.

1. Introduction

Rapid and accurate damage assessment is essential and crucial after disasters. The results of the post-disaster damage mapping provide useful information for the emergency situation and the disaster impacts and serve as a valuable tool for all agencies competent in disaster response, management and recovery. Especially during the first hours of the disaster emergency response phase, it is very important for the coordination of the executive and operational forces at central, regional and local level in order to rapidly and effectively respond to the

emergency needs of the affected population arising from the disaster.

In the past, mapping of disasters was generally a time consuming procedure, whose results were only available long after the disaster emergency response phase. Recent advances in technologies make it possible, much easier and faster for disaster researchers to collect and analyze data and to present and distribute critical information to civil protection agencies, the scientific community and the public, in near real time or real time always depending on the characteristics and the conditions of the disaster incidents. These new capabilities, considered as an evolution in disaster management, improve not only resource

* Corresponding author.

E-mail addresses: smavroulis@geol.uoa.gr (S. Mavroulis), eandreadk@geol.uoa.gr (E. Andreadakis), ns Spyrou@geol.uoa.gr (N.-I. Spyrou), vantonou@geol.uoa.gr (V. Antoniou), eskourt@geol.uoa.gr (E. Skourtsos), ppapadim@geol.uoa.gr (P. Papadimitriou), kassaras@geol.uoa.gr (I. Kassaras), gkaviris@geol.uoa.gr (G. Kaviris), gtselentis@geol.uoa.gr (G.-A. Tselentis), voulgaris@geol.uoa.gr (N. Voulgaris), pkary@tee.gr (P. Carydis), elekkas@geol.uoa.gr (E. Lekkas).

<https://doi.org/10.1016/j.ijdrr.2019.101169>

Received 25 September 2018; Received in revised form 15 April 2019; Accepted 23 April 2019

Available online 29 April 2019

2212-4209/ © 2019 Elsevier Ltd. All rights reserved.

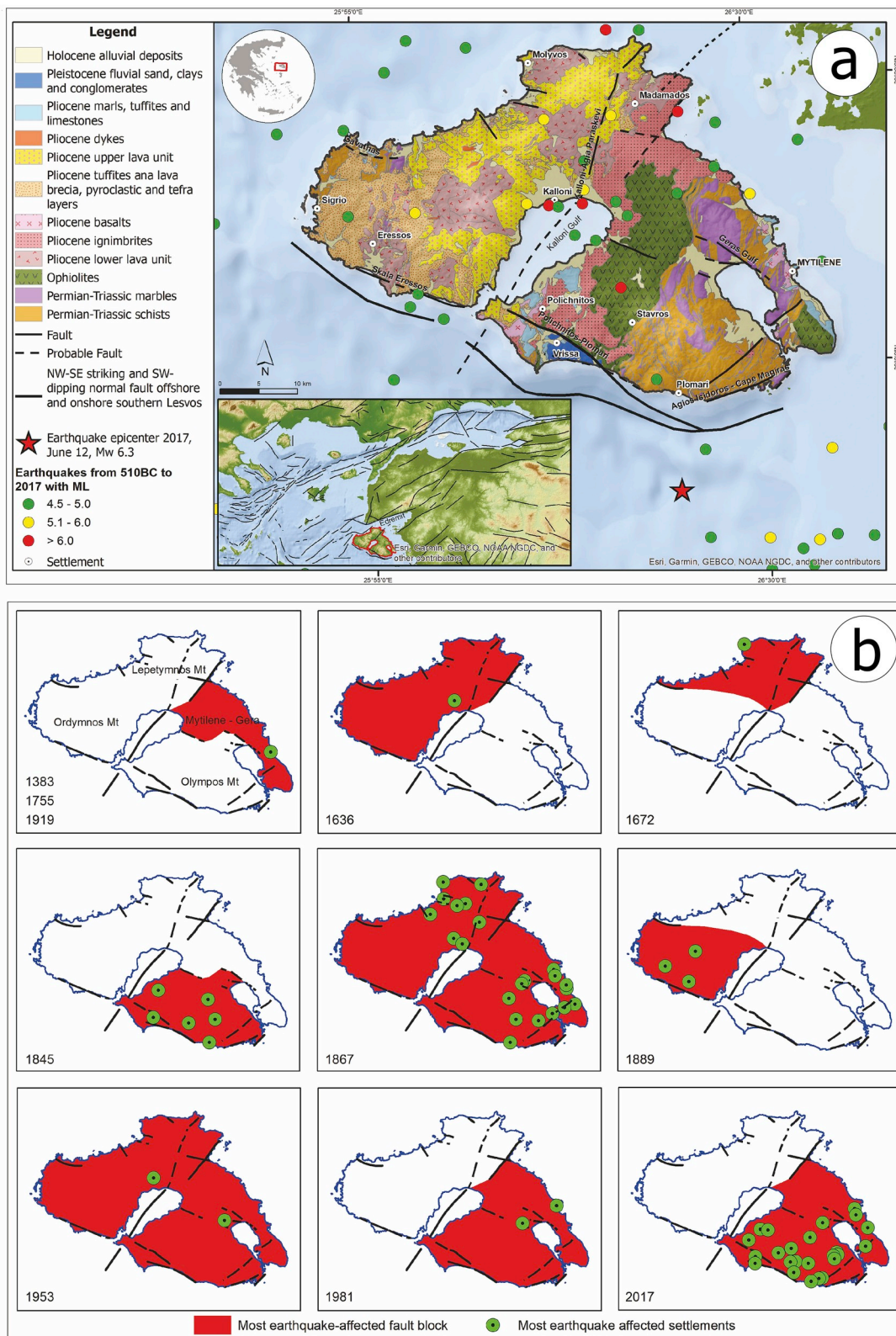


Fig. 1. (a) Simplified geological map of Lesvos. Vriasa, which is the 2017 Lesvos earthquake most affected area, is located in the hanging wall of Polichnitos fault and is founded on recent geological formations including Holocene alluvial deposits and Pleistocene formations. Significant historical and instrumentally recorded earthquakes and their epicenters that affected the geodynamic evolution of the North Aegean and Lesvos Island are also presented (Seismological data from Aristotle University of Thessaloniki Seismological Network, 2017 [25]; along with the 2017 Lesvos earthquake epicenter. (b) Areas with high contrasts in seismic intensities during major earthquakes in Lesvos. Green circles correspond to the most earthquake affected settlements of Lesvos Island. The maximum intensities have undoubtedly been observed in the southern and eastern part of Lesvos during the 1845, 1867, 1953 and 1981 earthquakes (data from Refs. [26–30] and references therein). (For interpretation of the references to color in this figure legend, the reader is referred to the Web version of this article.)

allocation and design of operations but also the safety of operators and the emergency responders themselves allowing accurate and precise delineation of the disaster-affected area.

Recently, the usability of Unmanned Aircraft Vehicles (UAV), commonly known as drones, has experienced significant growth and progress in disaster management as it has been clearly shown from various applications during post-disaster response and recovery operations [1–6]. As a result, an increasingly large number of applications are being developed including pre-disaster activity (prevention and early detection), activity immediately after the occurrence of a disaster (mitigation, monitoring and decision support) and the activity after the primary disaster elimination (quick assessment and recovery).

As regards earthquakes, the use of UAV is a fast and cost effective way for providing ultra-high resolution images of the affected area and conducting a rapid post-earthquake field survey. This approach is very important as it offers rapid: (a) assistance in search and rescue (SAR) operations by locating damaged infrastructures and scanning of buildings for survivors, (b) safe first building inspection and evaluation of damage degree, (c) assessment of the earthquake environmental effects (EEE), (d) identification of sites suitable for emergency shelters, (e) tracking displacement of affected population, (f) assistance of relief teams by transport of light equipment, devices and products as well as (g) mapping of newly established conditions for faster restoration and recovery (e.g. Refs. [7–11]; [6,12–14]).

Urban damage assessment seems to be a field with great potential [3,15,16] for many different disaster types including not only earthquakes [12,14,17], but also cyclones, typhoons and hurricanes [18,19]. A few more worth mentioning examples are use in humanitarian action in post-earthquake Haiti or post-hurricane Sandy [5], damage assessment and landslide mapping in Central Italy (Amatrice) earthquakes [6,20], flash flood magnitude assessment [21] and post-flash-flood mapping in Greece [22,23].

Along with the growth of the UAV, the web Geographic Information Systems (GIS) techniques and applications offer powerful tools to provide critical information and support decision making in disaster management. The advantages of the web GIS techniques during the post-earthquake response include: (a) immediate digital and online assessment of sites with EEE, (b) rapid first inspection of the earthquake damage induced on the building stock of the affected area, (c) real-time data transfer to laboratory for further processing and analysis and (d) free availability and accessibility to all agencies competent in civil protection and disaster management.

In the case of the June 12th, 2017 Mw 6.3 Lesvos (Northeastern Aegean, Greece) earthquake, building damage was observed in the southeastern part of the island with very heavy structural damage limited in the traditional settlement of Vrissa. Taking into account that Vrissa is located inland, further from the epicenter than other settlements with less damage, it looks like an earthquake impact paradox. For interpreting this paradox, a rapid field macroseismic reconnaissance was conducted performing not only the classical building-by-building inspection but also use of UAV and web GIS applications before any intervention in the settlement and with the highest possible detail.

The present study is a complete and comprehensive approach for earthquake-induced damage assessment in an area worst affected by an earthquake and it comprises integration of building-by-building inspection, use of desktop and web GIS applications, UAV survey (in-flight) and digital post processing (post-flight), extraction of data and information related to the buildings of the affected area, application of the European Macroseismic Scale 1998 based on the guidelines provided by Ref. [24] and assignment of macroseismic intensities and finally correlation of the all aforementioned data with the geological, geomorphological, geotechnical and seismological properties of the earthquake most affected area along with the characteristics and properties of buildings in the affected area. In this frame, the geological structure, the historical and instrumentally recorded seismicity of

Lesvos and the impact of significant historical and recent earthquakes on the natural and built environment of Lesvos Island are also presented. With this approach, an interpretation of the Vrissa earthquake impact paradox is attempted and the factors controlling damage and seismic intensities distribution throughout the settlement are also presented and analyzed.

2. Geological structure of Lesvos Island

The Lesvos Island is located in the northeastern Aegean, opposite to the coast of northwestern Asia Minor (Turkey) (Fig. 1a). The eastern part of the island comprises alpine rocks underlying tectonically large ultrabasic masses [31–36]; 1986 [37]; (Fig. 1a). The central part of the island is crossed by a series of paleo-volcanic centers operated during Lower Miocene and arranged in NE-SW direction resulted in extensive and thick volcanic rocks [37]. In the coastal region of southeastern Lesvos Lower Pliocene marls and limestones were deposited in lacustrine environment, which are crossed by or interbedded with small basaltic spills. On the contrary, in the coastal region of Vatera located in southern Lesvos (Fig. 1a), a relatively thick sequence of Pleistocene conglomerates and clays was deposited. The main active faults of Lesvos are the Gavathas, Skala Eressos, Kalloni - Agia Paraskevi, Polichnitos - Plomari, Agios Isidoros - Cape Magiras and Geras Gulf fault zones [38] (Fig. 1a). The most important tectonic structure in the 2017 earthquake-affected area is the NW-SE striking and SW-dipping Polichnitos fault (Fig. 1a), which constitutes the northern margin of the offshore southern Lesvos Basin characterized by numerous slumps and mass slides due to tilting of the basin margin [39]. The 2017 earthquake most-affected area is located northeast of Polichnitos fault (Fig. 1a).

3. Historical and recent seismicity, major earthquakes and intensity distribution

The region of Lesvos in the North Aegean Sea has suffered from several strong and destructive earthquakes since the antiquity, as well as during the 20th century [29,40,41]. Small earthquakes have been recorded in Lesvos except from Eressos area. By comparison of the areal distribution of epicenters with the tectonic structure of the island, it is concluded that all major faults accommodate seismic activity.

As regards the present-day seismotectonic setting of Lesvos, the island can be defined as tectonically and seismically active characterized by a high seismic activity [42]. Earthquake foci are shallow ($h \leq 50$ km) and concentrated in three zones with different magnitude ranges between ≤ 5.5 and 7.0 [45]. The first seismic zone crosses the northern coast of Lesvos with magnitudes varying from 6.0 to 7.0. The second seismic zone crosses the southern and southeastern coast of Lesvos with magnitudes varying from 5.0 to 6.0. The third seismic zone crosses the southwestern part of Lesvos with a NW orientation and magnitudes equal to or lower than 5.5. This is the most active fault zone of Lesvos.

Based on the historic and instrumentally recorded seismicity of Lesvos, it is concluded that the island has been repeatedly struck by earthquake with magnitude varying from 6.2 to 7.4 and seismic intensities of up to X [26–30] and references therein) (Fig. 1a) with significant effects to the local population, to the natural environment and the building stock of the island. It is not the first time that the southeastern Lesvos is the worst earthquake affected. Similar distribution of seismic intensities were also reported after the 1845 (October 11, $M = 6.8$, $I_{MAX} = X$), 1867 (March 7, $M = 7.0$, $I_{MAX} = X$), 1953 (March 18, $M = 7.4$, $I_{MAX} = IX+$) and 1981 (December 19, $M = 7.2$, $I_{MAX} = VIII$) earthquakes (Fig. 1b).

Based on the distribution of seismic intensities of historical and instrumentally recorded earthquakes in Lesvos wider area [26–30] and references therein), it is concluded that the highest seismic intensities have undoubtedly been observed in the southeastern Lesvos (Fig. 1b). On the contrary, the southwestern part of Lesvos has suffered low

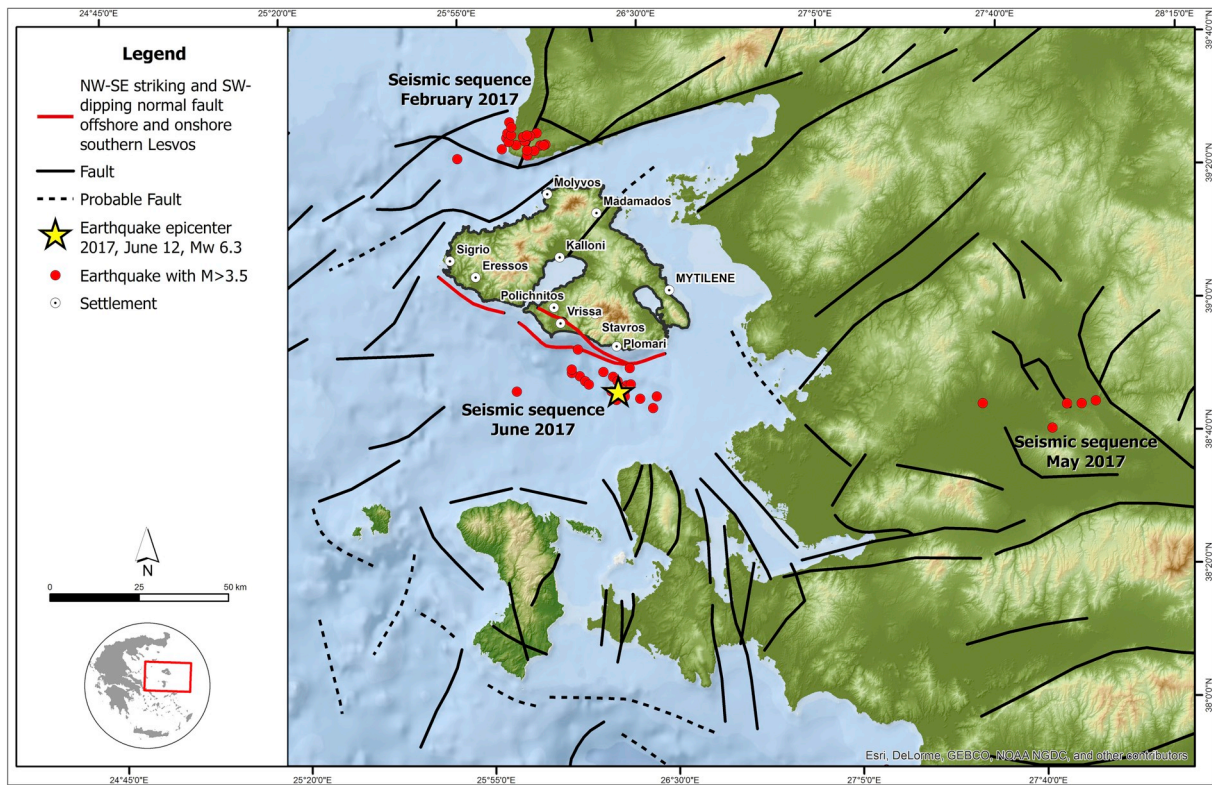


Fig. 2. In 2017, a significant seismic activity took place in the region of the NE Aegean and NW Asia Minor before the June 12, Mw 6.3. It comprised two seismic sequences. The first one was generated during February in the area north of Lesvos and the second one during May east of Lesvos. The majority of the seismic events were attributed to normal faulting as it is indicated by the focal mechanisms provided by Refs. [47,48].

seismic intensities (Fig. 1b).

The historical event that is quite similar to the 2017 Lesvos earthquake in terms of aerial distribution of earthquake-induced effects and assigned macroseismic intensities is the 1845 earthquake (October 11, $M = 6.7$, $I_{EMS-98} = 8.5$) according to Refs. [30,46]. This repeatability of the seismic effects infers local soil conditions that may have triggered local site amplifications of the seismic waves.

4. The June 12, 2017, Mw 6.3 Lesvos (Northeastern Aegean, Greece) earthquake

On June 12, 2017 (12:28 GMT, 15:28 local time) an Mw 6.3 earthquake struck Lesvos Island (Northeastern Aegean, Greece) [47]. It was predominantly felt on Lesvos Island and throughout the North Aegean Islands and western Turkey. It claimed the life of a woman due to building collapse and 15 injured due to collapsing buildings and falling debris. The southeastern part of Lesvos Island suffered the most by the earthquake in its natural environment, building stock and infrastructure.

The earthquake epicenter has been determined offshore southeastern Lesvos (Fig. 2). The focal depth of the earthquake has been estimated at about 13 km. The fault plane solutions demonstrated a NW-SE striking and SW-dipping normal fault bounding the offshore Lesvos basin located between Lesvos and Chios islands [47].

The aftershock sequence of the Lesvos earthquake from 12 to 20 June included about 308 events [47; Fig. 2). Six events had magnitude equal to or larger than 4.0, with the largest of them occurred five days later at 19:50 local time and measured Mw 5.3 [46]. The focal mechanism of the largest aftershock indicated a NE-SW strike-slip fault which is not consistent with the causative tectonic structure of the main earthquake [47,48].

The 2017 Lesvos earthquake induced extensive secondary EEE comprising ground cracks and slope movements resulting in damage to

the road network and adjacent building structures and related facilities. A small tsunami wave of peak-to-peak amplitude of ~ 30 cm was generated offshore southeastern Lesvos and was observed in Plomari port [46].

Based on the analysis of the rupture history of the main shock by inversion of teleseismic P-wave records by considering a slight modification of the CMT fault plane solution [46], suggested that the main rupture area was ~ 11 km long and ~ 6 km wide and the maximum seismic slip was of ~ 9 cm, while close to the surface the slip ranged from 1 to 3 cm. The rupture duration was found ~ 7 s, while the released seismic moment was calculated equal to $\sim 2.5 \times 10^{18}$ Nm. Based on the main shock rupture analysis, rupture directivity was indicated towards NW [46], where the worst affected villages are founded and the maximum seismic intensities are assigned.

Two important seismic sequences were preceded the June 12, 2017 Mw 6.3 Lesvos earthquake (Fig. 2). The first one started on the morning of the February 6th, 2017 and was located north of Lesvos Island (Fig. 2). It continued until the end of the same month comprising 20 seismic events with $M \geq 3.5$ [25] and caused heavy damage on buildings of at least five villages and 5 injured residents. Based on seismological data recorded and provided by the European-Mediterranean Seismological Centre (EMSC, <https://www.emsc-csem.org/Earthquake/252/Earthquake-sequence-in-Western-Turkey>) for the period from February 6th to 13th, the first seismic sequence comprised 4 events with $M \geq 5.0$, 16 events with $M \geq 4.0$, 126 events with $M \geq 3.0$ as well as 967 events with $M \geq 2.0$. It is significant to note that all epicenters were generated in short time period and limited space with width of about 20–30 km (Fig. 2). The second seismic sequence started with an M 5.1 earthquake generated southeastwards of Lesvos and comprised aftershocks with magnitude ranging from M 4.3 to 4.9 generated on the same day [25] (Fig. 2).

As far as the 2017 Lesvos earthquake impact on buildings is concerned, damage was localized in the western part of the affected area

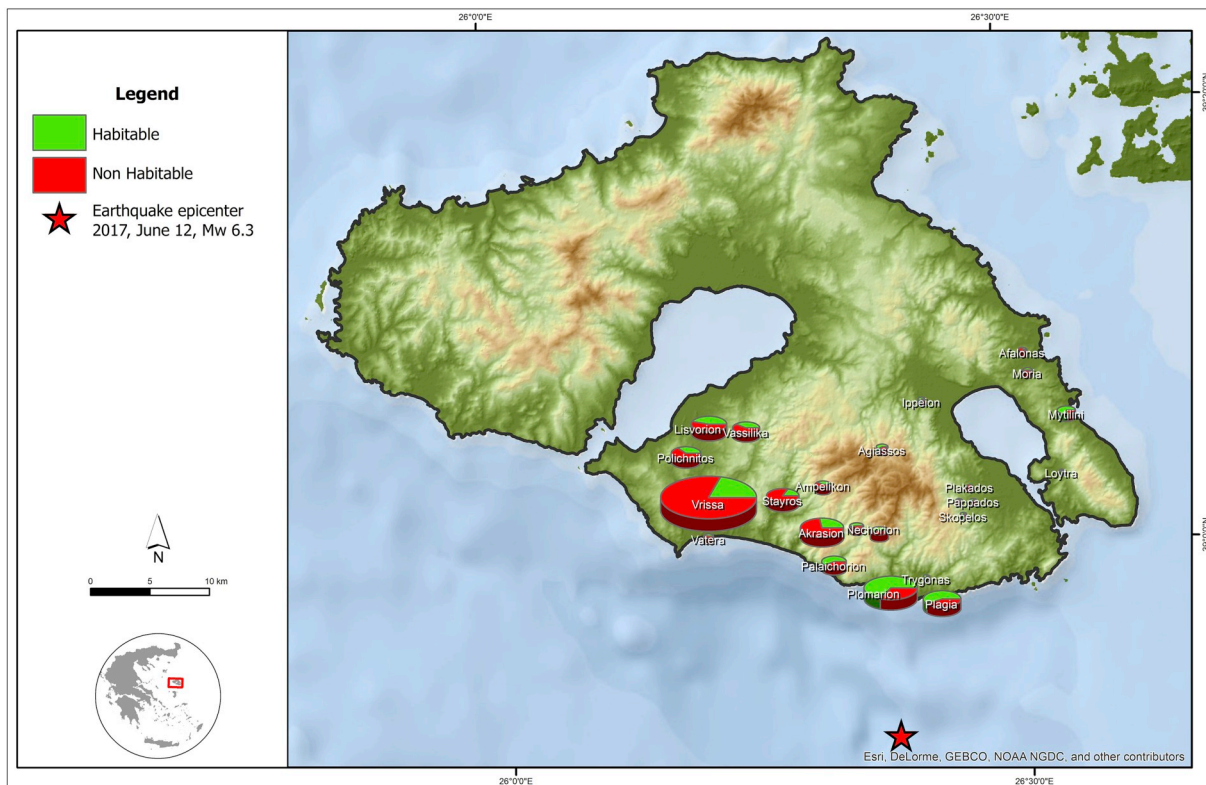


Fig. 3. Percentage of damage per settlement of the southeastern part of Lesvos. Vrisa, Plomari, Akraasi, Plagia, Lisvori, Stavros and Polichnitos are the most affected villages of the affected area. Especially, the traditional settlement of Vrisa was devastated by the earthquake and concentrated the 50% of the non-habitable buildings inspected by the [49].

(Fig. 3). Minor damage was also reported from other localities of Chios Island located southwards as well as from localities of western Turkey.

According to data provided by the [49]; 1115 buildings in 29 settlements of the southeastern part of Lesvos (Fig. 3) were characterized as non-habitable including 976 residential buildings, 41 business premises, 39 temples and public buildings as well as 59 warehouses. More specifically, in Vrisa, 113 buildings were characterized as habitable, while 472 structures including 408 residential buildings, 25 business premises, 6 temples and public buildings as well as 33 warehouses were characterized as non-habitable. Based on the aforementioned data, it is concluded that almost 50% of buildings that suffered damage are concentrated in Vrisa settlement (Fig. 3).

5. Macroseismic data acquisition

5.1. General approach

Taking into account the areal distribution of damage induced by the 2017 Lesvos earthquake in the southeastern part of the island and the fact that Vrisa is located further inland from the epicenter than other settlements with less damage (e.g. Plomari, Vatera etc) (Fig. 3), Vrisa seemed like an earthquake impact paradox. Moreover, the first reports, apart from the earthquake effects on human health (fatality and injuries), referred to severe damage including total or near total collapses of many buildings throughout the village.

The research team arrived at the site during the first hours of the disaster response phase and decided to conduct a rapid macroseismic reconnaissance throughout the devastated Vrisa performing not only classical methods of earthquake damage assessment (e.g. building-by-building inspection), but also modern and innovative techniques, which comprise the use of UAV and web GIS applications as the basis of a rapid post-earthquake damage assessment before any intervention was made in the settlement. Thus, all earthquake effects on the natural

environment and the building stock of Vrisa were captured and saved with maximum accuracy for further processing and analysis.

5.2. Building-by-building inspection using GIS desktop and online applications

The building-by-building inspection was done in more than 1000 buildings throughout Vrisa. The collected macroseismic data comprised type of structure, vulnerability class, type of damage and damage grade for each building. All buildings were added as points or polygons to analog maps and the relative macroseismic data were recorded to registration forms specially designed for the needs of the survey. After the completion of the field survey, the analog maps were scanned, converted to digital form, georeferenced, digitized and converted from raster to vector form in GIS environment in order to extract the areal distribution of the earthquake damage, assign seismic intensities based on the application of the EMS-98 and realize the various factors controlling the damage grade and distribution.

In order to manage the building-by-building inspection, both desktop (ArcMap v. 10.5) and online (www.arcgis.com) ArcGIS platform was used because, although it is a commercial software, it provides many advantages, such as many analysis tools, online availability of data and open source code ready-made web applications (Fig. 4), all in the same software. The use of free software was also possible, but it needed more time to process the data, more than one software and code writing skills, all unavailable at that time, due to the urgent character of the macroseismic study.

Collection and organization of existing vector and grid data along with their spatial and descriptive analysis was made, through a geodatabase containing all available information layers and also new ones for collecting data during field survey, including all the necessary fields for the descriptive information. The pre-existing information layers include coastline, settlements, geological formations and tectonic

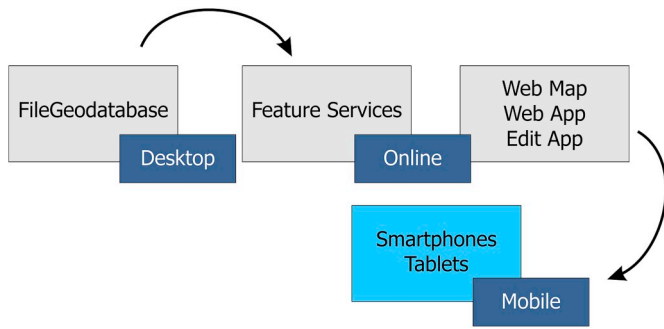


Fig. 4. Workflow needed to be done in order to use mobile devices for collecting data via Collector for ArcGIS application.

structures comprising faults of Lesvos Island. Because of the urgent character of this macroseismic study during the first hours of the disaster response phase, only one editable information layer was created for field macroseismic data collection. It was a point vector file, which included spatial information, description, audiovisual material that consisted of photos or videos for each collected point as well as the field group and the time of data acquisition.

In order for these information layers to be accessed online, they were uploaded, transformed accordingly and added to a web map where individual parameters for each of the information layers including symbols, appearance or not of tags and pop-up menus among others [50,51] were customized. Moreover, refresh interval was defined for the information layer regarding data collection. Specific symbols for each user group were created, so that each group can directly be identified. Available imagery was defined as background of the aforementioned information layers.

Using the web map, a web application was created. Mobile devices

(e.g. smartphones, tablets) but also any available browser could access the created web map and therefore information layers in real time. The individual parameters of the application, such as color appearance, availability or not of searching information in the layers as well as location tracking, were also defined. Last but not least, both web map and the corresponding web application were responsive, meaning that were adapting on the displaying screen of each user. Access to this app was only given to the administrator and to the members of the scientific field teams, in order to have all the available information in their mobile screen, to facilitate their work during data collection, to give them access to check each other's work in real time conditions and for the administrator, to inspect the whole procedure and guide them through, keeping in mind that the whole undertaking was taking place few hours after the earthquake.

For real time dissemination purposes, a story map was created. All collected pre-processed macroseismic data were available to ministries, state authorities, agencies competent in civil protection and disaster management as well as in the direction and coordination of the executive and operational forces at central, regional and local level.

At this point, although the story map was publicly available, dissemination focused only to rapidly inform these agencies about the prevailing conditions, in the context of investigating the effectiveness of such an application for rapidly and effectively respond to the emergency needs of the affected population arising from the earthquake disaster. Taking into account that the official field teams responsible for damages recording needed more than a week to complete the task, the 1-day implementation needed to select, create, process the information layers, create and customize the web apps, collect data and disseminate the results in real time, became a serious reason to pressure the responsible agencies to change the still existing classical way of collecting data in case of a disaster. Also, many if not all agencies had their own credentials to access the ArcGIS platform, so, if requested, it was easy to

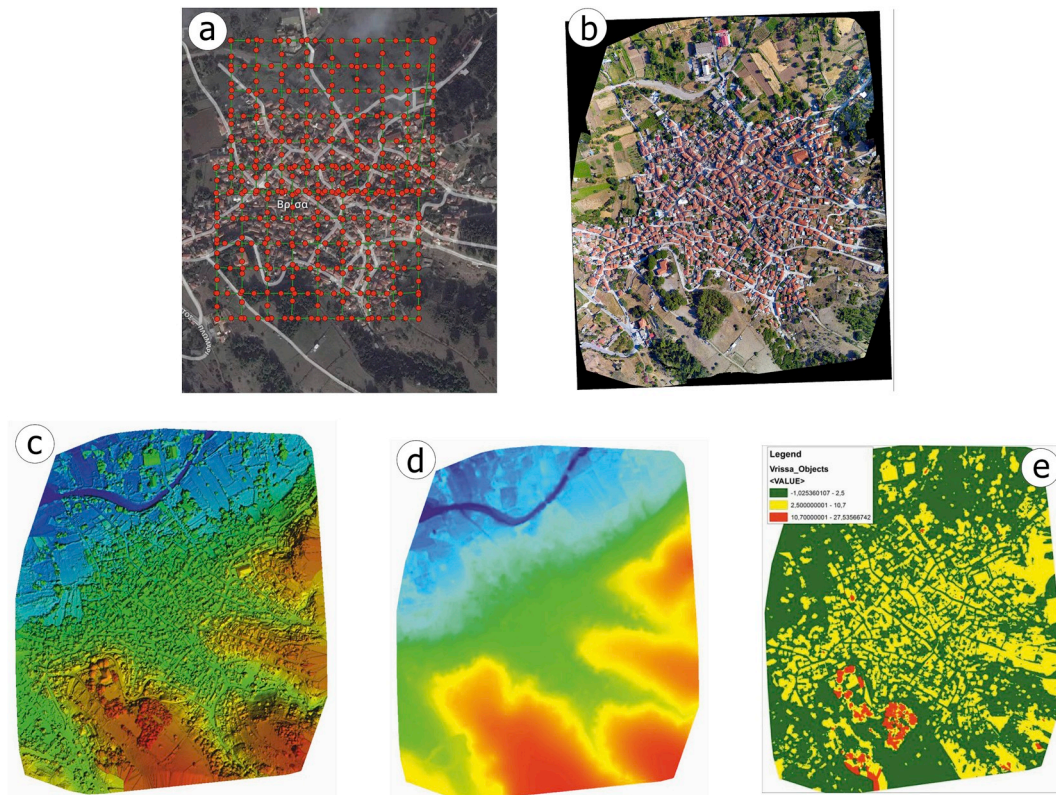


Fig. 5. (a) The flight plan was designed to cover the whole area of the affected settlement. It was carried out along two sets of paths with perpendicular alignment and 439 images were acquired. (b) The Orthomosaic, (c) the Digital Surface Model (DSM) and (d) the Digital Terrain Model (DTM) of the affected settlement. (e) The extracted polygons derived from the extraction of DTM from DSM.

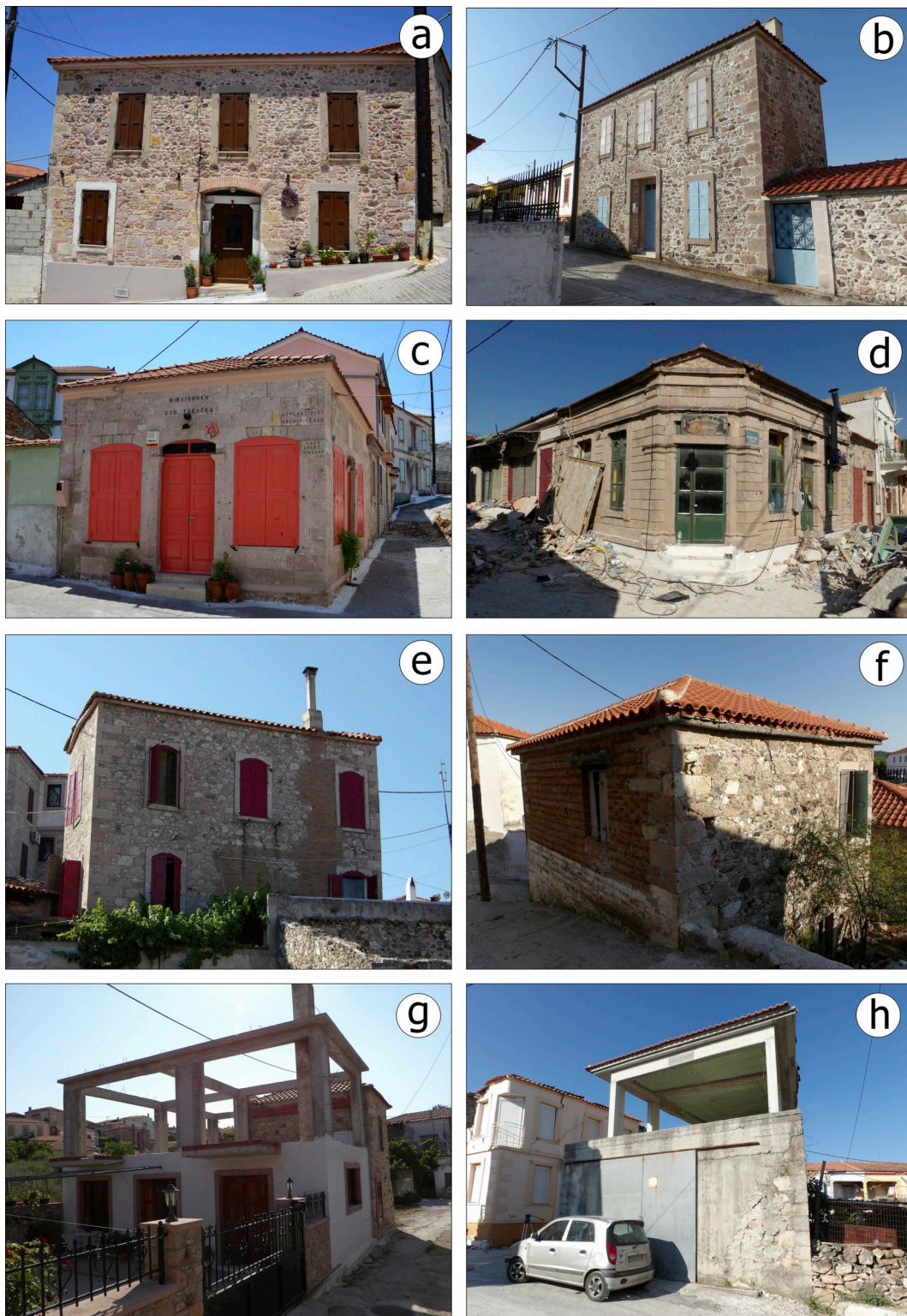


Fig. 6. The dominant building types in Vrissa comprise masonry buildings (a–f) and R/C buildings (g–h). The masonry buildings constitutes the majority of the building stock of Vrissa. They mainly include massive stones (a–d) and mixed types including mainly massive stones and perforated bricks (e, f). Their construction is dated back to the late 19th or early 20th century after repeated destructive earthquakes of the 18th century and more specifically from 1845 to 1889. The R/C buildings (g, h) comprise an R/C frame with infill and partition walls.

be able to change or alter the database's scheme in the editable information layer, in order to add more descriptive information according to their needs. This would be a good start to establish a digital database scheme compatible with the data needed to be collected in corresponding disasters.

5.3. UAV post-earthquake disaster survey (in-flight)

The UAV post-earthquake disaster survey took place in the field shortly after the earthquake and during the first hours of the disaster response phase along with the building-by-building inspection, so that

the disaster scene was almost intact by demolition processes and rubble management. An Unmanned Aircraft System was deployed comprising a DJI Phantom 4 Pro UAV, a ground controller, an iPad and a Pix4D capture software and the following steps were followed:

The flight plan was designed to cover the whole area of the settlement. Pix4D capture was used to create a suitable 3D map flight plan (Fig. 5a). Two consecutive flights specially designed for 3D modelling were executed to collect imagery (Fig. 5a). The scanning of the earthquake-affected settlement was carried out along two sets of paths with perpendicular alignment, at a height of 90 m above ground in the area of interest. The flight areas were overlapping in order to be inter-calibrated. 439 images of Vrissa were taken and were used as an input for further processing in the Pix4D Mapper Pro software.

5.4. Digital post processing (post-flight) and verification of field survey data

In the first phase of modeling, the 439 acquired images were processed in the Pix4D mapper software and more than 14500 matches were produced per image. The 3D model of the settlement was produced, along with the orthomosaic (Fig. 5b), the Digital Surface Model (DSM) (Fig. 5c) and the Digital Terrain Model (DTM) (Fig. 5d) of the area, expanding over 0.367 km², with an average ground sampling distance of 4.14 cm. Then, the DSM was introduced to ESRI ArcMap and through raster filtering of differences between DSM and DTM, building polygons were obtained (Fig. 5e).

It is significant to note that Vrissa is a traditional settlement over a century old, also declared as preserved according to the respective decree of the Governmental Gazette of Hellenic Republic. This means that architecture is quite uniform and buildings have certain architectural features. This uniformity essentially enables the classification of objects into groups based on their shape and their height and the extraction of the similar buildings.

Taking into account the aforementioned, the resulting raster after subtracting DTM from the DSM contained only recognizable objects, which were then grouped into three groups, and more specifically building height between 2.5 and 10.7 m, shorter than 2.5 m and taller than 10.7 m. Then, adjusting the histogram of the objects raster, large trees, poles, etc. were excluded, resulting in a raster containing all building surfaces and some of the trees, which were then converted to polygons shapefile in ArcGIS.

6. Application of the EMS-98 for the most affected area of the 2017 Lesvos earthquake

6.1. The EMS-98 review

The EMS-98 considers three categories of effects: (a) on humans, (b) on objects and on nature and (c) on damage to buildings [24]. In comparison to previous scales, the differentiation of structures (buildings) into vulnerability classes (A to F) along with the classification of earthquake-induced building damage into damage grades (1–5) are the main advantages of the EMS-98. It is predominantly used in Europe [52] for the Mw 6.0 1999 Athens (Greece) earthquake [53], for the Mw 6.3 2009 L' Aquila (Italy) earthquake [54], for the 2008 Andravida (Northwestern Peloponnese, Greece) earthquake [55], for the 1986 Kalamata (Southwestern Peloponnese, Greece) earthquake [56], for the early 2014 Cephalonia (Ionian Sea, Greece) earthquakes] and often-times worldwide [43,44] for the Mw 7.9 2008 Wenchuan (China) earthquake [57], for the Mw 7.1 2010 and Mw 6.3 2011 New Zealand earthquakes [58], in the Asia-Pacific region [59], for the Mw 7.8 2015 Nepal, Gorkha earthquake among the most characteristic applications] as there are no serious limits for applying EMS-98 at an international level [60].

6.2. Architectonic character, dominant building types and differentiation of buildings into vulnerability classes in Vrissa

The dominant building types of the affected area are (a) masonry buildings, (b) reinforced-concrete (R/C) buildings, and special structures including (c) monumental structures and (d) industrial structures.

The first most prevalent category includes 1- to 3-storey masonry buildings with load-bearing walls (Fig. 6a–f). These structures can be further classified depending on the construction material of the masonry, which can be composed of (a) massive stones (Fig. 6a–b), (b) manufactured stone units (Fig. 6c–d), (c) mixed materials including massive stones, manufactured stone units, handmade solid clay bricks, perforated bricks and concrete blocks (Fig. 6e and f). These materials were bound by different types of mortar including mainly clay and lime mortars, but after recent and extensive retrofit and strengthening, the old traditional mortar was replaced by cement mortar.

In order to assign a vulnerability class to the aforementioned masonry buildings, the following facts were taken into account.

Based on various sources comprising archaeological findings and historical records (e.g. Refs. [61–63]), Vrissa was founded on its present site on the late 19th century. The masonry buildings observed in Vrissa have been constructed in one of the most seismically and tectonically active areas of the Eastern Mediterranean. Moreover, their majority has been built during the late 19th and the early 20th century, i.e. after a period of time during which Lesvos has been repeatedly struck by destructive earthquakes. More specifically, in 1845, 1865, 1867, 1886, 1889 and 1919 with significant impact on the built environment comprising heavy structural damage, as it has been clearly shown by detailed analysis of the historical seismicity of Lesvos [26–30,45] and references therein; [40,41].

As a result, more effective antiseismic construction techniques were developed and applied to buildings after each destructive earthquake. These earthquake-resistant constructions as well as the repair and retrofitting of buildings existed as a way of prevention and mitigation against the destructive earthquake effects on buildings from the early 19th century or earlier.

Moreover, the time interval between the aforementioned earthquakes is very small, of the order of 2, 20 and 30 years. These periods are very smaller than the average life span of a generation. Thus, construction workers and builders had the opportunity to learn from their mistakes revealed after an earthquake. They also had the ability to transfer the knowledge and cumulative lessons to successor workers of the next generations. In contradiction, when the recurrence interval between two destructive earthquakes are larger than the average life span of a generation, then the collective memory of construction workers and builders is either composed more of historical events than of actual memories or totally erased.

This fact resulted in decreased primary seismic vulnerability of buildings in the affected area of southeastern Lesvos, due to the fact that those dealing with the building construction had the opportunity to improve their construction methods as well as construction materials and earthquake resistant methodologies and technology.

A fact that verifies the truth of the abovementioned is the observation of antiseismic structures in Vrissa village. During the post-earthquake building-by building inspection conducted in the 2017 Lesvos earthquake affected area, anti-seismic construction techniques and systems that present significant differences from the conventional traditional building practices of the Northeastern Aegean were detected throughout Vrissa village.

More specifically, many buildings have constructed with dual structural system. The structures employ both autonomous masonry walls and timber frames with extensive “X” bracing (Fig. 7). During an earthquake, these frames could guarantee the stability of the roof in case of a partial collapse of the masonry structure. This building system seems to be based on advanced structural principles, such as that of energy dissipation. Thus, it represents one of the earliest surviving

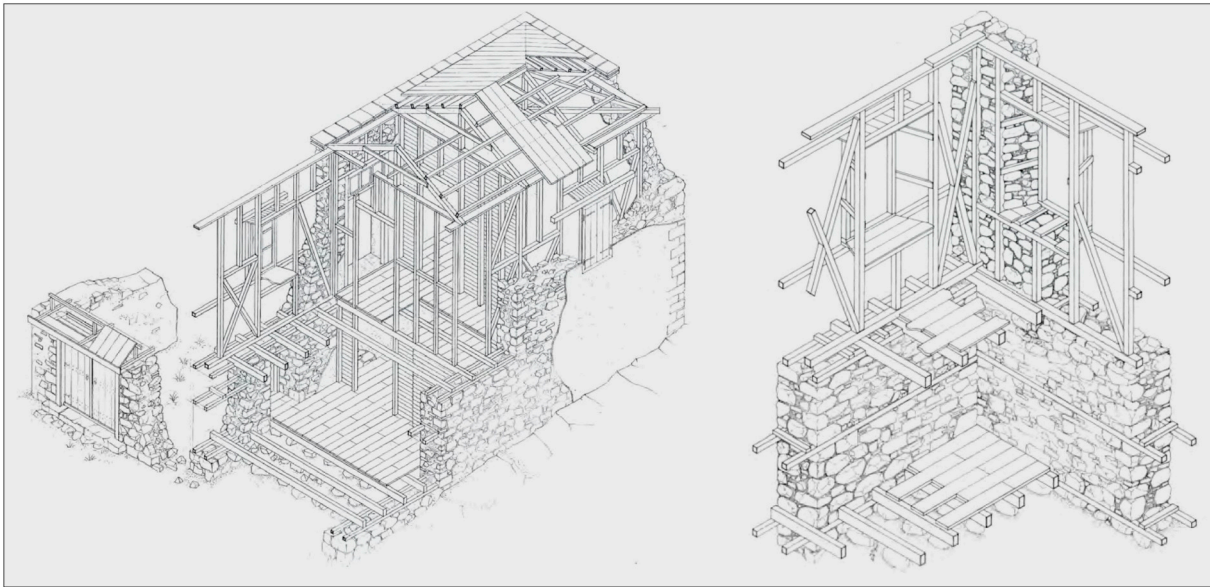


Fig. 7. Axonometric section of a traditional two-storey residential building with dual structural system comprising masonry walls and the supporting wooden frame (from Ref. [64]).

architectural antiseismic responses to earthquake motion in Greece and Turkey. It has been also observed in Eressos settlement in the western part of Lesbos and in Bergama in the western coast of Turkey and thoroughly described and analyzed by Refs. [64,65].

These buildings are 2-storey structures with total height not exceeding 6 m and with rectangular plan of about 4×10 m (Fig. 7). The ground floor is composed of clay stone masonry reinforced with timber frames on many levels and is characterized by few openings, while the upper floor comprises clay stone masonry with self-supported timber frames include many windows without the structure losing its robustness. Both structural systems support the roof and are both connected with the base of the building (Fig. 7).

In case of heavy cracking or partial collapse of the stone masonry walls resulting in decreased seismic capacity of the building, the wooden frame is able to safely sustain vertical loads of the upper floor. Thus, the structure does not collapse, remains safe and gives residents time for the repair or reconstruction of the severely damaged masonry. During the 2017 earthquake, such buildings with dual structural system located in the worst affected area showed good structural performance with large cracks and partial collapse of the masonry structure, while the wooden structure successfully sustained the earthquake loads (Fig. 7).

These characteristics of the constructions in Vrissa led to the adoption of a governmental gazette of the Hellenic Republic on the characterization of Vrissa as a traditional settlement and of its buildings as preserved structures. As a result, all buildings of Vrissa were recently and extensively maintained, repaired, retrofitted or strengthened with various methods and techniques in the frame of a large project before the generation of the 2017 Lesbos earthquake including traditional wall reinforcement, replacement of the old traditional mortar by cement mortar, covering of the exterior and the interior surface of masonry walls by resistant plasters increasing resistance of the building, use of metal tie-rods and anchor plates for reinforcement and replacement of all old roofs in order to increase the structural stability of the buildings. Moreover, based on this governmental gazette, the change of use in these buildings, which requires major interventions in their structural and non-structural elements (e.g. demolition of walls), is prohibited. Thus, these preserved structures are more protected from alterations and interventions that can negatively affect their antiseismic response.

From the results of the post-earthquake building-by-building inspection, the buildings in Vrissa are characterized by small openings,

large piers between openings and quoins as well as walls with perpendicular stiffening. All these characteristics contribute to more resistant buildings with great strength in Vrissa.

It is also significant to note that Lesbos is an island with many natural resources and a strong naval tradition and history dating back to the depths of antiquity. In a similar way, many seafarers' families active in the high seas and dominating the sea trade for many years lived in Vrissa. This economic prosperity of the inhabitants of Vrissa is reflected in their residential buildings and their monumental structures. In particular, their houses were constructed with the best building materials of their time and with good practices that improved their antiseismic behavior and not with loose materials and bad practices that would negatively affect the stability of the building.

Based on the integration of all abovementioned data, it is concluded that the vast majority of buildings in Vrissa, although masonry and historical constructions, are designed and constructed in such a way to successfully sustain the disastrous effects of an earthquake, which at that time was a frequent and destructive phenomenon. They are not just simple stone masonry buildings classified as of vulnerability class B, but well-designed and well-constructed masonry buildings, with great strength and increased seismic resistance and therefore they can be classified as buildings of vulnerability class C (Table 1; Fig. 8).

The second category includes R/C buildings with R/C frame and infill walls (Fig. 6g and h). They are recent structures built during the last decades according to strict anti-seismic regulations and specifications and belong to the vulnerability class D (Fig. 8). The R/C frames consist of beams (horizontal elements) and columns (vertical elements), which are connected by rigid joints. These R/C structures are cast monolithically and more specifically beams and columns are cast in a single operation in order to act in unison. The R/C frames are resistant to both lateral and gravity forces and loads through bending of horizontal and vertical elements. It is significant to note that all new building structures in Lesbos are designed on the basis of a PGA equal to 0.24 g corresponding to the second largest seismic strength demand based on the Greek seismic code for earthquake resistant structures [66].

The third category include masonry monumental structures such as churches and schools. Regarding the church construction and architecture in Lesbos, there are few well-preserved and still-standing monuments, mainly of the one-aisled basilica type, representing the church architecture of Lesbos before the 18th century. They are

Table 1
Building types in Vrissa settlement and differentiation of buildings into vulnerability classes.

Type of structure	Characteristics	Vulnerability class based on the EMS-98
Masonry structures, with randomly placed stones	Unreinforced buildings with load-bearings walls composed of randomly placed stones often bound with mortars of poor and inadequate quality, dated back to the late 19th and early 20th centuries	B
Masonry structures, with massive stone	Unreinforced buildings with load-bearings walls composed of stonework comprising massive stones often bound with mortars of poor and inadequate quality, dated back to the late 19th and early 20th centuries	C
Masonry structures, with manufactured stone units	Unreinforced buildings with load-bearings walls composed of stonework comprising manufactured stone units often bound with mortars of poor and inadequate quality, dated back to the late 19th and early 20th centuries	C
Masonry structures, with mixed building material	Unreinforced buildings with load-bearings walls composed of stonework comprising massive stones, manufactured stone units, clay bricks and fragments often bound with mortars of poor and inadequate quality, dated back to the late 19th and early 20th centuries	C
Masonry structures with RC floors	Buildings with load-bearings walls composed of stonework comprising massive stones, manufactured stone units, clay bricks and fragments and reinforced-concrete floors	C
Reinforced-concrete structures	Reinforced-concrete buildings with structural frame characterized by moderate level of earthquake-resistant design (ERD)	D

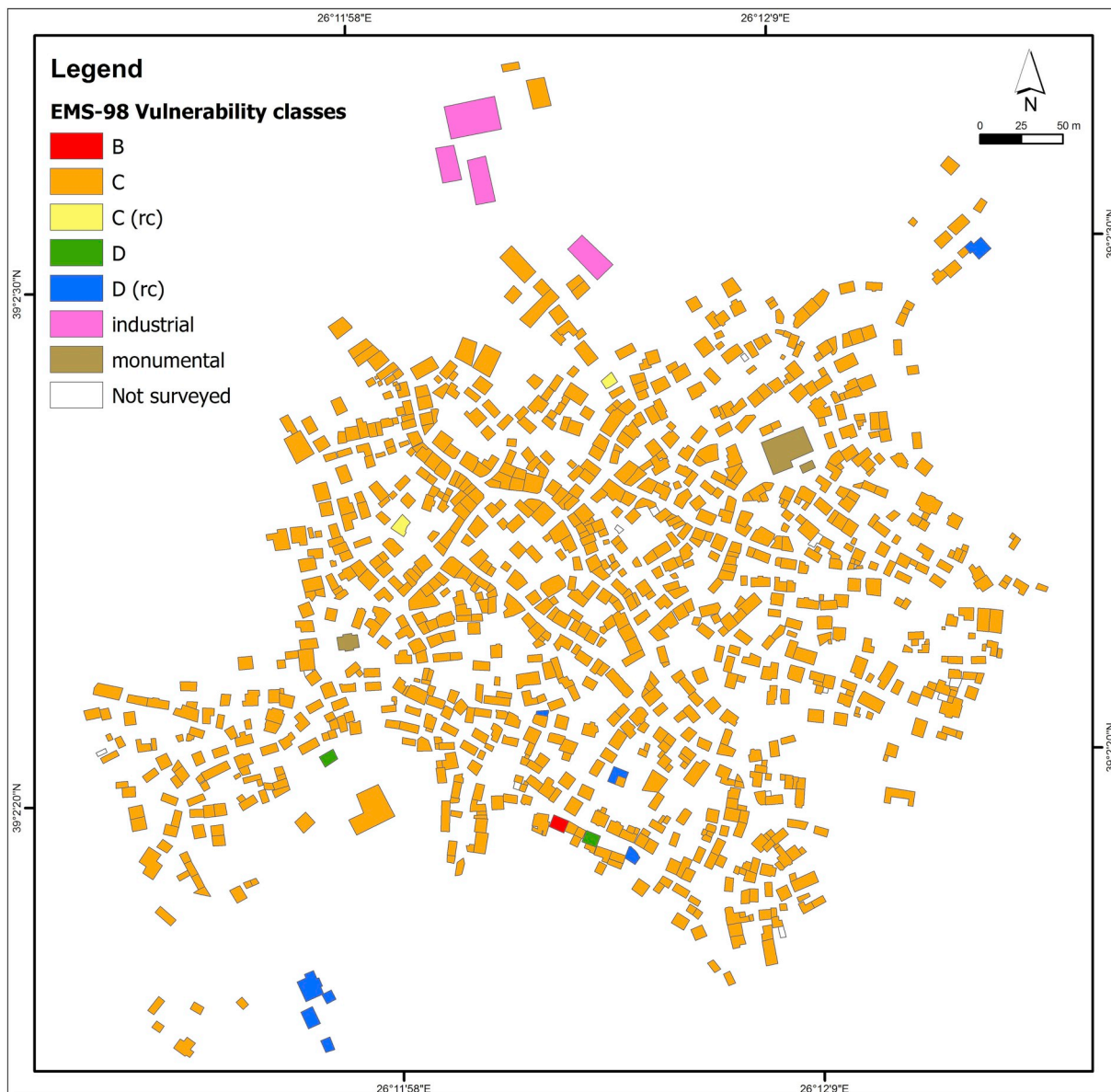


Fig. 8. Map of the buildings' vulnerability in Vrissa settlement based on the field macroseismic observations and the EMS-98. A percentage of 99.38% of the buildings are of vulnerability class C.

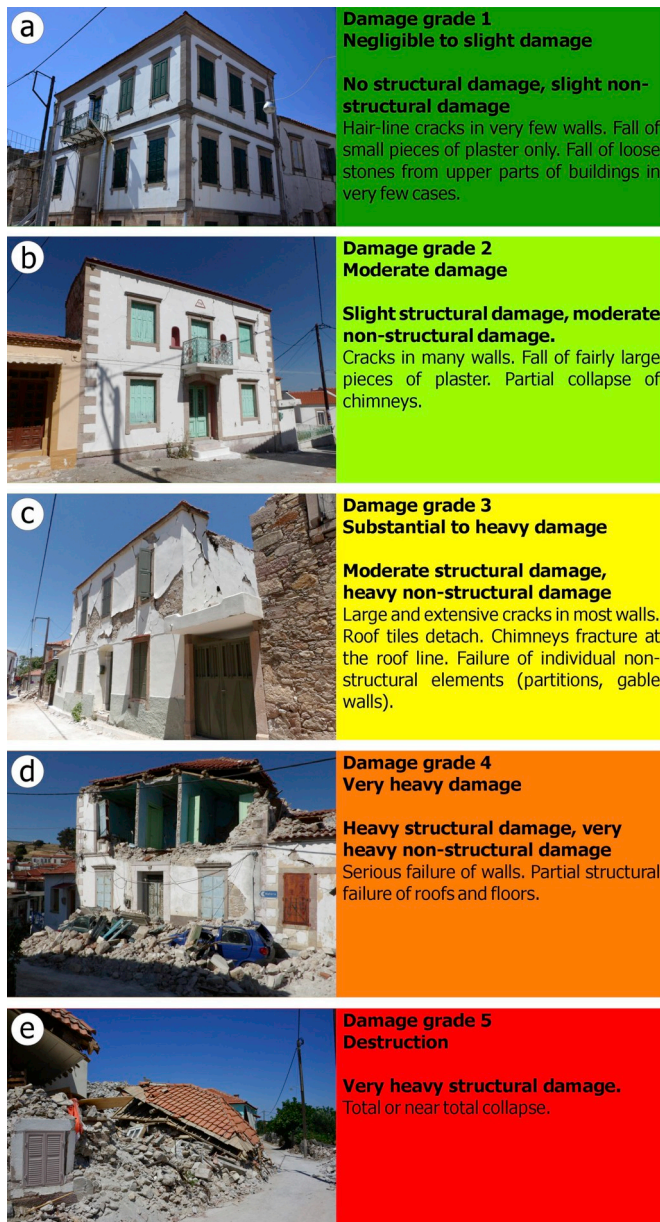


Fig. 9. Masonry buildings suffered the most by the 2017 Lesvos earthquake. The observed damage grades varied from 1 (a) to 5 (e). The classification of damage to masonry buildings is based on the EMS-98.

characterized of small size, simplicity of the exterior appearance and subtle interior space. Detailed information on building materials, construction methods and architectural design of this period are scarce. This fact is attributed to the high seismicity of the North Aegean region especially during the 19th century and the occurrence of destructive earthquakes from 1845 to 1889, the high vulnerability of these structures due to poor and inadequate construction materials and absence of anti-seismic protection design and measures.

The fourth category include industrial buildings including production structures and their masonry chimneys. They are defined as architectural monuments. They are still standing, although their static compliance is gradually reduced through the years.

6.3. Damage and its classification into damage grades

The masonry buildings suffered the most by the 2017 Lesvos earthquake. They sustained (a) damage grade 1 (negligible to slight



Fig. 10. Special structures including churches, industrial buildings and their masonry chimneys as well as schools suffered heavy damage from the 2017 Lesvos earthquake. Churches suffered damage including large cracks in various parts such as walls (a–e) and the dome, detachment of large pieces of plaster from load-bearing masonry walls (a, b, c, e), dislocation and fall of several roof tiles (e) and partial collapse of load-bearing masonry walls (c, d, e). Masonry industrial buildings in Vrissa suffered large cracks and partial collapse of their masonry walls (f) and large cracks of their masonry chimneys on the verge of collapse (g). School buildings suffered damage varying from fall of the gable over the main entrance (h) and cracks in their masonry walls (i, j) to partial collapse (k).

damage) comprising hairline cracks in the load-bearing masonry walls (Fig. 9a), (b) damage grade 2 (moderate damage) including cracks in many walls, detachment of small pieces of places from the walls and partial collapse of chimneys (Fig. 9b), (c) damage grade 3 (substantial to heavy damage) comprising large and extensive cracking of all masonry load-bearing walls, detachment of large pieces of plaster in all load-bearing walls, dislocation and fall of roof tiles, detachment of the



Fig. 11. (a–d) Traditional residential buildings with dual structural system including masonry walls and timber frames with extensive “X” bracing in Vrissa settlement (a–d). During an earthquake, these frames could guarantee the stability of the roof in case of a partial collapse of the masonry structure. This dual structural system represents one of the earliest surviving architectural responses to earthquake motion in Greece and Turkey and was also observed in Eressos and Bergama by Refs. [64,65]. (e–f) The R/C buildings showed good performance and remained almost intact (e) by the 2017 Lesvos earthquake. But there were exceptions (f) including cracks in the infill walls, detachment of large pieces of plaster from the infill walls of the ground floor as well as detachment of the infill wall from the surrounding RC frame.

roof from the rest of the structure and fall of gables (Fig. 9c), (d) damage grade 4 (very heavy damage) including heavy structural failure of roofs and floors (Fig. 9d) and (e) damage grade 5 of partial and total collapse (Fig. 9e).

The special structures including temples, post-byzantine structures, museums, schools and industrial buildings with masonry load-bearing walls suffered similar damage with the masonry residential buildings. More specifically, temples suffered damage comprising cracks in most of the masonry walls (Fig. 10a and b) and in other parts such the dome, the columns, the aisles, the apse and the gable. Post-byzantine structures suffered the aforementioned damage as well as partial collapse of the walls (Fig. 10c–e).

Industrial buildings suffered partial collapse of the perimeter masonry walls and damage of the masonry chimneys on the verge of collapse (Fig. 10f and g). A typical example is the industrial building located at the northern entrance of Vrissa settlement comprising an oil-mill along with its masonry chimney (Fig. 10f and g). The main building is composed of masonry load-bearing walls built with roughly treated stones and handmade solid clay bricks, while the masonry chimney has been built with solid clay bricks (Fig. 10f and g). Unfortunately, both structures were abandoned since the late 90s, but they were typical examples and reminders of the industrial prosperity of Vrissa during the late 19th century.

Schools suffered fall of the gable above the entrance and partial collapse of the load-bearing masonry walls (Fig. 10h–k).

As regards traditional buildings with the dual structural system, they performed better than the masonry structures with load-bearing walls. The primary structural system comprising the masonry walls of the ground floor sustained no structural damage and light non-structural damage including cracks of the masonry (Fig. 11a–d). The secondary structural system showed good performance during the earthquake sustaining successfully the vertical loads of the upper floor and resulting in still standing residential buildings after the earthquake, despite the fact that the masonry suffered damage varying from large cracks to partial collapse (Fig. 11a–d).

All R/C buildings constructed during the last decades showed good performance during the 2017 Lesvos earthquake since none of them suffered heavy structural damage. R/C buildings suffered only non-structural damage including cracks in the infill walls, detachment of large pieces of plaster from the infill walls and detachment of the infill walls from the surrounding R/C frame (damage grade varying from 1 to 2 based on the EMS-98) (Fig. 11e and f). However, some free standing elements sensitive to base accelerations were dislocated and damaged.

Taking into account the aforementioned macroseismic data, among structures constructed without seismic provisions, the stone masonry residential buildings, monumental and industrial structures suffered the

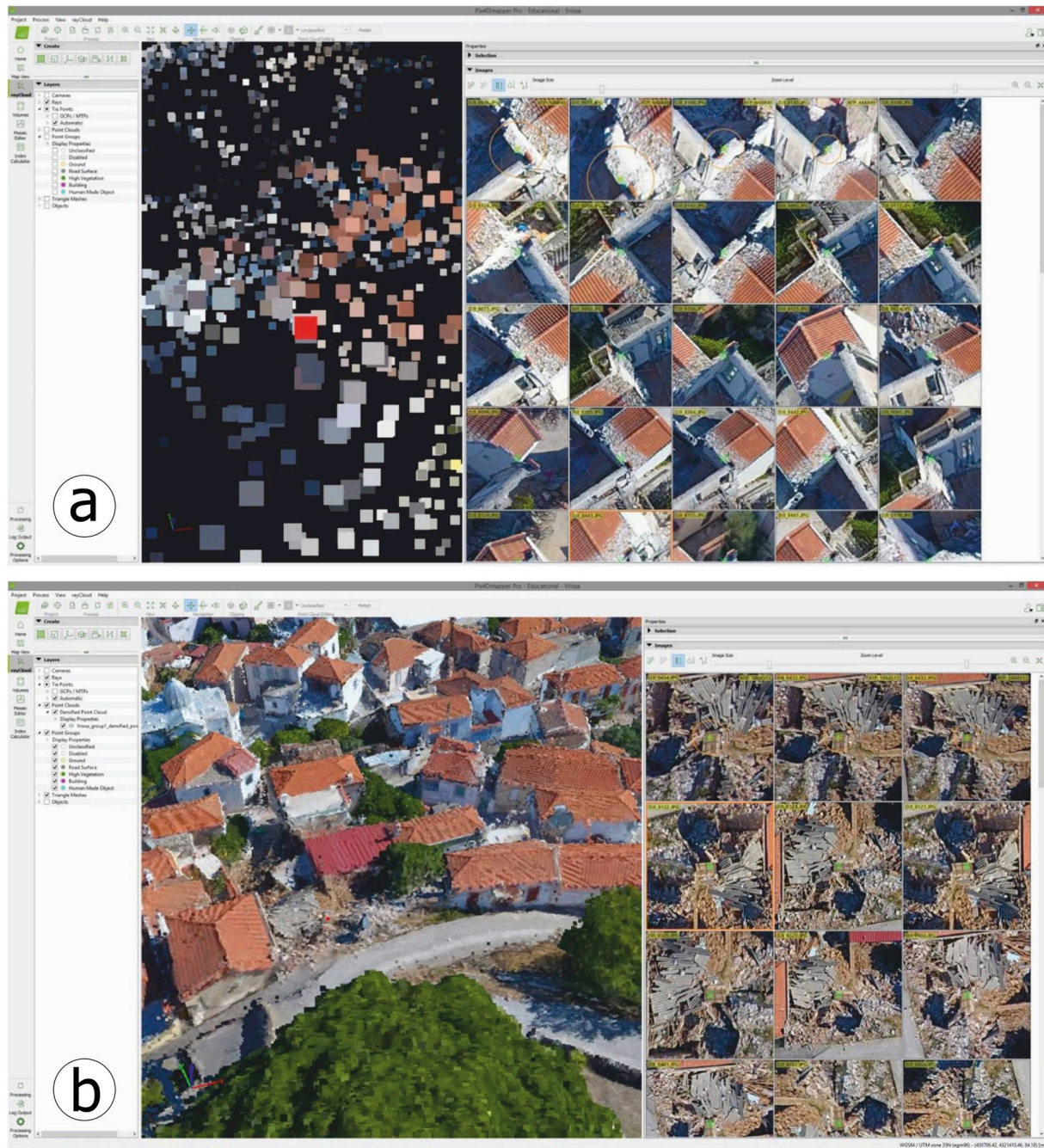


Fig. 12. Building inspection with multiple points of view through Pix4D environment.

most by the earthquake, while the traditional buildings of the area with dual structural system performed relatively well and suffered minor damage. R/C buildings remained intact by the earthquake.

6.4. The EMS-98 isoseismal map of the 2017 Lesvos earthquake most affected area and a methodology for isoseismal maps drawing

The field observations including vulnerability classes, building damage and damage grades based on the EMS-98 application were verified for accuracy by revisiting the site through the acquired 3D model produced in previous step of the applied methodology and by using all footage available for any point on demand, in Pix4D (Fig. 12). All polygons were finally attributed with a unique number, a code description referring to the building type, a vulnerability class and a damage grade. A vulnerability map (Fig. 13a) and a damage grade map

(Fig. 13b) were produced based on the buildings polygon and their attributes.

After the differentiation of buildings into vulnerability classes and the classification of damage into damage grades, the compilation of an isoseismal map is the next step in order to draw a complete and clear image of the earthquake impact on the built environment.

Almost all buildings (99.38%) in Vrissa belong to vulnerability class C. Consequently, the attempt to determine the macroseismic intensity can only be based on the statistical processing of vulnerability class C buildings across the different intensity values. On the basis of the definitions of quantity [24], the minimum and maximum percentages of damaged buildings for each intensity degree were set.

In order to create a map of spatial distribution of damage grade of vulnerability class C buildings throughout the settlement, weighted point density was calculated using building centroids, having assigned

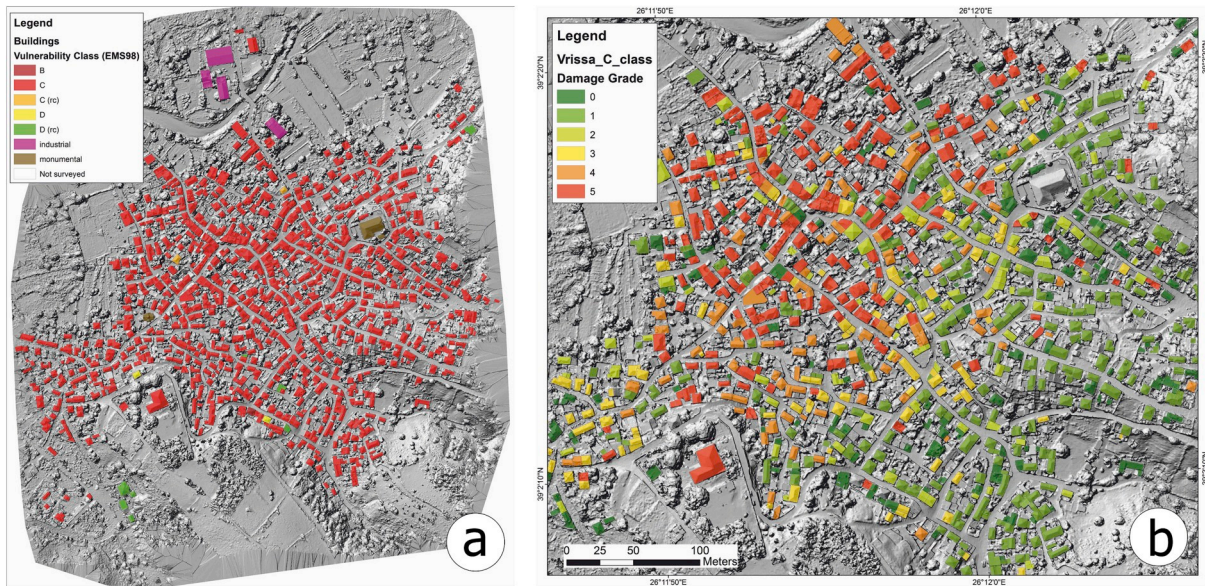


Fig. 13. (a) Vulnerability class and (b) damage grade maps of Vrissa settlement based on the EMS-98.

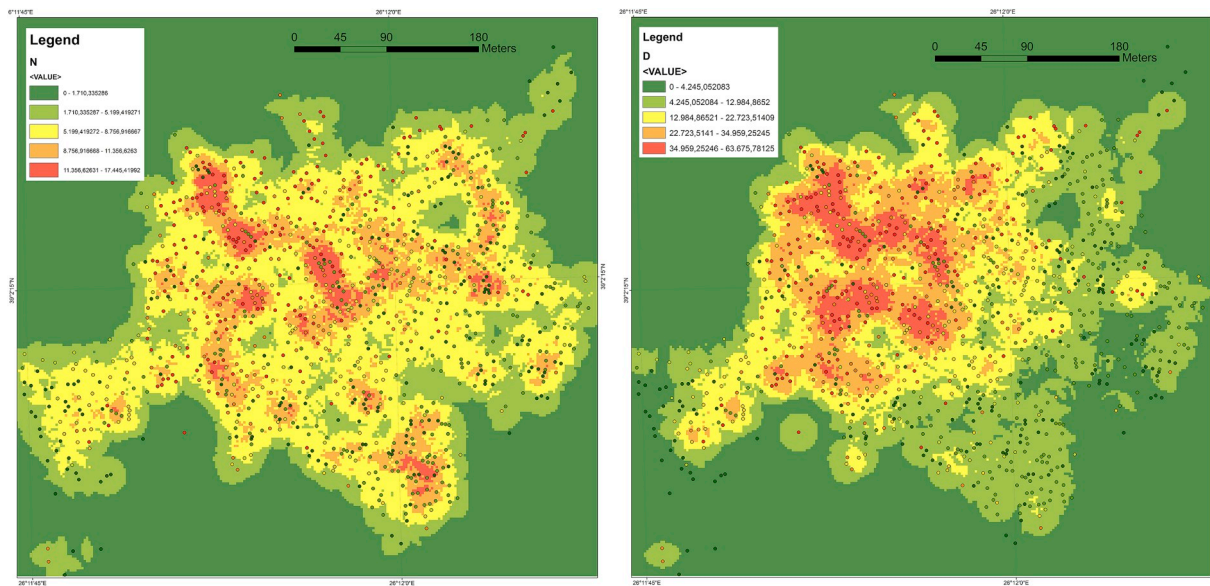


Fig. 14. These two maps depict for every pixel a value of N (point density of buildings in the pixel neighborhood) (left) and D (point density of damage in the pixel neighborhood) (right).

the damage grade that each building suffered. Calculations provide the magnitude per unit area from point features around a neighborhood around each cell. The search radius defines how detailed or generalized the raster output will be (larger search radius, more generalized raster). Neighborhood was considered a circular area in that radius. At any given pixel of the area, buildings are counted within the search radius and weighted with the damage grade (e.g. one building of damage grade 3 will count three times and result in a value of 3, one building of damage grade three and two buildings of damage grade 2 will result in a value of $1 \cdot 3 + 2 \cdot 2 = 7$, etc, following the function $D = \frac{\sum(n \cdot d)}{\pi r^2}$, where D is the damage grade per unit area for each pixel, n is the number of building centroids within the search radius suffering damage grade d . The search radius r was set to the default value, that is, one thirtieth of the larger dimension of the building area extent (19.10 m). The results are shown in Fig. 14.

For every EMS-98 intensity value, a minimum and a maximum percentage of buildings of each vulnerability class, suffering specific

damage grades is considered characteristic (Table 2). These percentages, applied on the D values, can provide the thresholds of D values for each intensity value.

Furthermore, building point density was calculated and spatially analyzed, $N = \frac{\sum(n)}{\pi r^2}$, where N is the number of buildings per square kilometer. In this way, the two maps depict for every pixel a value of D (point density of damage in the pixel neighborhood) and N (point density of buildings in the pixel neighborhood) (Fig. 14). These two values divided (D/N), provide an estimated damage grade for vulnerability class C buildings, for every pixel (Table 2, columns 8 and 9).

Having calculated the spatial distribution of this value, the thresholds of D values for every intensity value are transformed into D/N thresholds. Applying these thresholds to the classification of D/N values on the map, there is a direct match with intensity values I_{EMS} . The thresholds of D/N values for EMS intensity values from VII to XII were subsequently calculated, as shown in Table 2.

The resulting classification thresholds are represented in the chart

Table 2
Minimum and Maximum Damage Score as a function of building point density, and Weighted Damage Grade, independent of Building Point Density, for each Intensity Degree (VII-XII, descending).

Damage Grade	House Centroid Density N (n/km ²)	Damage points D(n*d/km ²)	Minimum Percentage for XII _{EMS98}	Maximum Percentage for XII _{EMS98}	Minimum Damage Score for XII _{EMS98}	Maximum Damage Score for XII _{EMS98}	Minimum Weighted Damage (Minimum D/N) for XII _{EMS98}	Maximum Weighted Damage (Maximum D/N) for XII _{EMS98}
0	1000	0					98	98
1	1000	1000					4	5
2	1000	2000						
3	1000	3000						
4	1000	4000						
5	1000	5000	80%	100%	4000	5000		

Damage Grade	House Centroid Density N (n/km ²)	Damage points D(n*d/km ²)	Minimum Percentage for XI _{EMS98}	Maximum Percentage for XI _{EMS98}	Minimum Damage Score for XI _{EMS98}	Maximum Damage Score for XI _{EMS98}	Minimum Weighted Damage (Minimum D/N) for XI _{EMS98}	Maximum Weighted Damage (Maximum D/N) for XI _{EMS98}
0	1000	0					98	98
1	1000	1000					1	4
2	1000	2000						
3	1000	3000						
4	1000	4000	60%	100%	2400	4000		
5	1000	5000	20%	60%	1000	3000		

Damage Grade	House Centroid Density N (n/km ²)	Damage points D(n*d/km ²)	Minimum Percentage for X _{EMS98}	Maximum Percentage for X _{EMS98}	Minimum Damage Score for X _{EMS98}	Maximum Damage Score for X _{EMS98}	Minimum Weighted Damage (Minimum D/N) for X _{EMS98}	Maximum Weighted Damage (Maximum D/N) for X _{EMS98}
0	1000	0					98	98
1	1000	1000					0	2,4
2	1000	2000						
3	1000	3000						
4	1000	4000	20%	60%	800	2400		
5	1000	5000	0%	20%	0	1000		

Damage Grade	House Centroid Density N (n/km ²)	Damage points D(n*d/km ²)	Minimum Percentage for IX _{EMS98}	Maximum Percentage for IX _{EMS98}	Minimum Damage Score for IX _{EMS98}	Maximum Damage Score for IX _{EMS98}	Minimum Weighted Damage (Minimum D/N) for IX _{EMS98}	Maximum Weighted Damage (Maximum D/N) for IX _{EMS98}
0	1000	0					98	98
1	1000	1000					0	1,8
2	1000	2000						
3	1000	3000	20%	60%	600	1800		
4	1000	4000	0%	20%	0	800		
5	1000	5000						

Damage Grade	House Centroid Density N (n/km ²)	Damage points D(n*d/km ²)	Minimum Percentage for VIII _{EMS98}	Maximum Percentage for VIII _{EMS98}	Minimum Damage Score for VIII _{EMS98}	Maximum Damage Score for VIII _{EMS98}	Minimum Weighted Damage (Minimum D/N) for VIII _{EMS98}	Maximum Weighted Damage (Maximum D/N) for VIII _{EMS98}
0	1000	0					98	98
1	1000	1000					0	1,2
2	1000	2000	20%	60%	400	1200		
3	1000	3000	0%	20%	0	600		
4	1000	4000						
5	1000	5000						

Damage Grade	House Centroid Density N (n/km ²)	Damage points D(n*d/km ²)	Minimum Percentage for VII _{EMS98}	Maximum Percentage for VII _{EMS98}	Minimum Damage Score for VII _{EMS98}	Maximum Damage Score for VII _{EMS98}	Minimum Weighted Damage (Minimum D/N) for VII _{EMS98}	Maximum Weighted Damage (Maximum D/N) for VII _{EMS98}
0	1000	0					98	98
1	1000	1000					0	0,4
2	1000	2000	0%	20%	0	400		
3	1000	3000						
4	1000	4000						
5	1000	5000						

showing I_{EMS} vs D/N (Fig. 15).

A second method of neighborhood analysis was used, applying the Kernel density approach (ceteris paribus). A smoothly curved surface is fitted over each point. The surface value is highest at the location of the point and diminishes with increasing distance from the point, reaching zero at the Search radius distance from the point. The volume under the surface equals the Population field value for the point, or 1 if NONE is specified. The density at each output raster cell is calculated by adding

the values of all the kernel surfaces where they overlay the raster cell centre. The kernel function is based on the quadratic kernel function described.

In this approach, in a random sample of size n from a random variable with density f, the kernel density estimate of f at the point x is given by the equation $\hat{f}_h(x) = \frac{1}{nh} \sum_{i=1}^n K\left(\frac{x-X_i}{h}\right)$, where the smoothing parameter h is known as the bandwidth and the kernel K is generally chosen to be a unimodal probability density symmetric about zero [67].

The results of the point density and the Kernel density are very similar.

The results compared to the previous analysis are very similar (Fig. 16). Simple point density results in a more fragmented map, while Kernel density provides smoother and more generalized contours as well as a more comprehensive map for the viewer (Fig. 16).

6.5. Factors controlling the type and the distribution of building damage

Taking into account the overall post-earthquake scene in Vrissa, the characteristics and properties of the affected structures and the spatial distribution of damage within the settlement, it is concluded that same structures with same construction, same building materials and same vulnerability presented different structural and non-structural damage within the same settlement and in small distances.

More specifically, it is concluded that its western part is the worst affected characterized by damage grades 4 and 5 (Fig. 17) including partial structural failure of roofs, floors and walls as well as total or near total collapse respectively. 47.2% of the surveyed buildings of vulnerability class C suffered damage grade 5, 18.1% grade 4, 12.7% grade 3, 8.0% grade 2 and 13.3% grade 1. On the other hand, the eastern part remained relatively undamaged with the observed damage grades varying from no damage at all to damage grade 2 (Fig. 17).

Apart from the most affected western part of Vrissa founded on alluvial deposits, very heavy structural damage including partial or total collapses was also observed in isolated areas in its southwestern intact part. The most characteristic “damage islet” has been detected around the partially collapsed elementary school of Vrissa (Fig. 17). It is characterized by partial or total collapse of masonry buildings as well as by damage to infrastructures and more specifically to the road and electricity networks.

It is obvious that the damage grade observed in the western part of Vrissa and within the damage islets cannot be justified by the properties and the vulnerability of the buildings, but it can be attributed to several factors.

Taking into account the geological and tectonic structure, the geomorphological setting and our field macroseismic observations on the type, vulnerability and damage grades of buildings, it is concluded that the worst affected part of Vrissa is founded on Holocene alluvial deposits comprising gray and red clays, sands and gravels, while the slightly affected part is founded on Pleistocene deposits including fluvial sands, clays and conglomerates with thickness of about 100 m. Moreover, the groundwater level in the alluvial deposits was high resulting in reduction of (a) the absorption of the vertical (P) waves, (b) the strength and the stiffness of the soils due to the fact that the water acts as lubricant reducing friction and increasing mobility of deposits and (c) the generation of the S waves due to saturated deposits.

Another fact that could lead to the increase of damage to buildings and respective higher seismic intensities is the probable generation of stationary waves in the area comprising alluvial deposits, multiple reflection of seismic waves not only in sedimentary layers but also in the contact between different geological formations (e.g. Holocene alluvial and Pleistocene deposits). As regards the transition from the devastated part to the relatively intact part of Vrissa, there is a very narrow transition zone with abrupt change from slight to very heavy structural damage.

The damage islets are attributed to earthquake-induced landslide

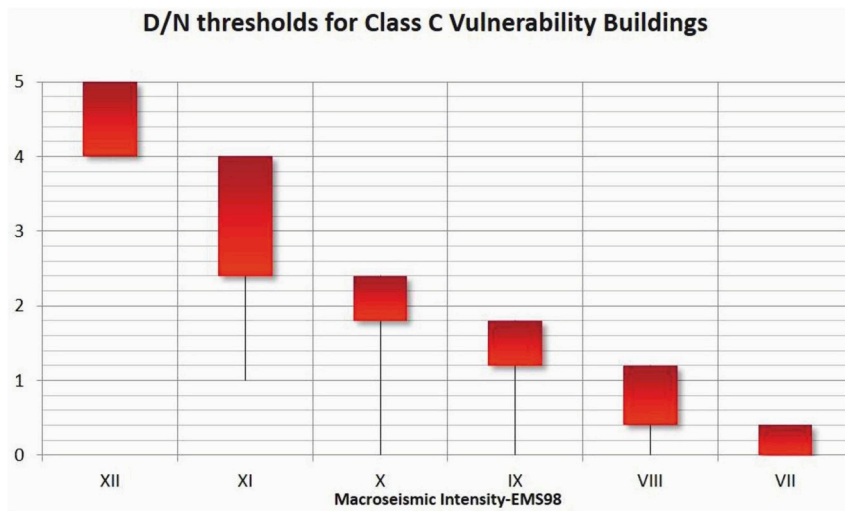


Fig. 15. D/N thresholds for buildings of vulnerability class C.

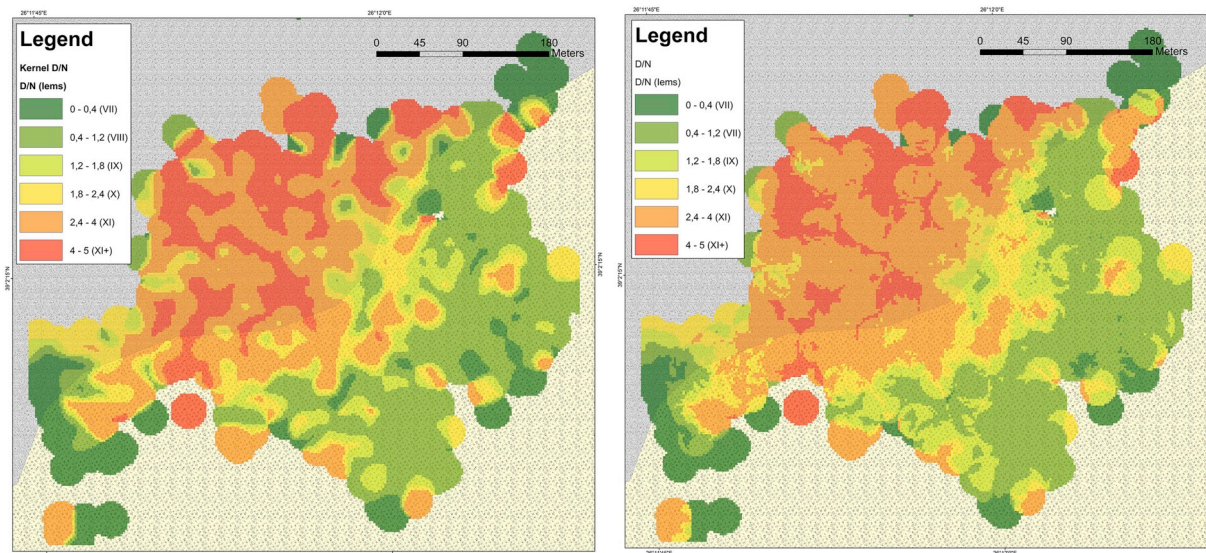


Fig. 16. Kernel density (left) vs Point density (right) results of neighborhood analysis. Kernel density calculates on the basis of a Gaussian distribution around the point and not around the point per se. Results are almost the same, but smoother and more comprehensible with Kernel density.

phenomena along a geotechnically unstable zone detected south of the elementary school of Vrissa and characterized by relatively steeper slopes (Fig. 17). A landslide was generated southeast of the school resulting in destruction of the road network and tilting and collapse of electricity pillars. Another landslide was observed in the southern part of the school resulting in hairline cracks to a masonry perimeter wall located in the westward prolongation of the crown cracks, partial collapse of a retaining wall supporting the school’s playground and severe damage to a warehouse adjacent to the unstable and mobilized slope inside the school’s yard. It is significant to note that this is not the first time that landslides have been generated in the same site. Evidences of generation of similar phenomena (creep and slow crack growth) were detected on an adjacent perimeter wall that suffered cracks and were repeatedly restored with the use of concrete.

Based on data and results of this field macroseismic survey after the June 12, 2017 Lesvos earthquake and geological reconnaissance in the most affected area of Vrissa, it is concluded that the geological setting comprising recent deposits, the occurrence of geotechnically unstable zones, the geotechnical properties of the foundation soils and the building characteristics in the devastated village have been identified as the main factors affecting and defining the areal distribution of building

damage in Vrissa settlement. More specifically, the occurrence of buildings founded on alluvial deposits, along geotechnical unstable zones and on slopes in an area that it is bounded by significant faults in combination with the near-field location of Vrissa and observed rupture directivity phenomena detected by Refs. [46,68] led to large differences in damage grades and seismic intensities between the western and eastern part of Vrissa.

7. Conclusions – discussion

In this study, an integration of real-time field, aerial and web-based methodologies, data and information is applied in the 2017 Lesvos earthquake most affected area during the immediate response phase in order to assess the earthquake impact on the natural and built environment of the study area, to rapidly and effectively distribute this critical information to all agencies competent to the disaster management and to correlate damage with the geological structure, the geotechnical properties, the building characteristics of the affected area.

The applied approach comprised a rapid-post-earthquake building-by-building inspection, support and enhancement of the inspection by means of both GIS desktop and GIS online applications as well as UAV

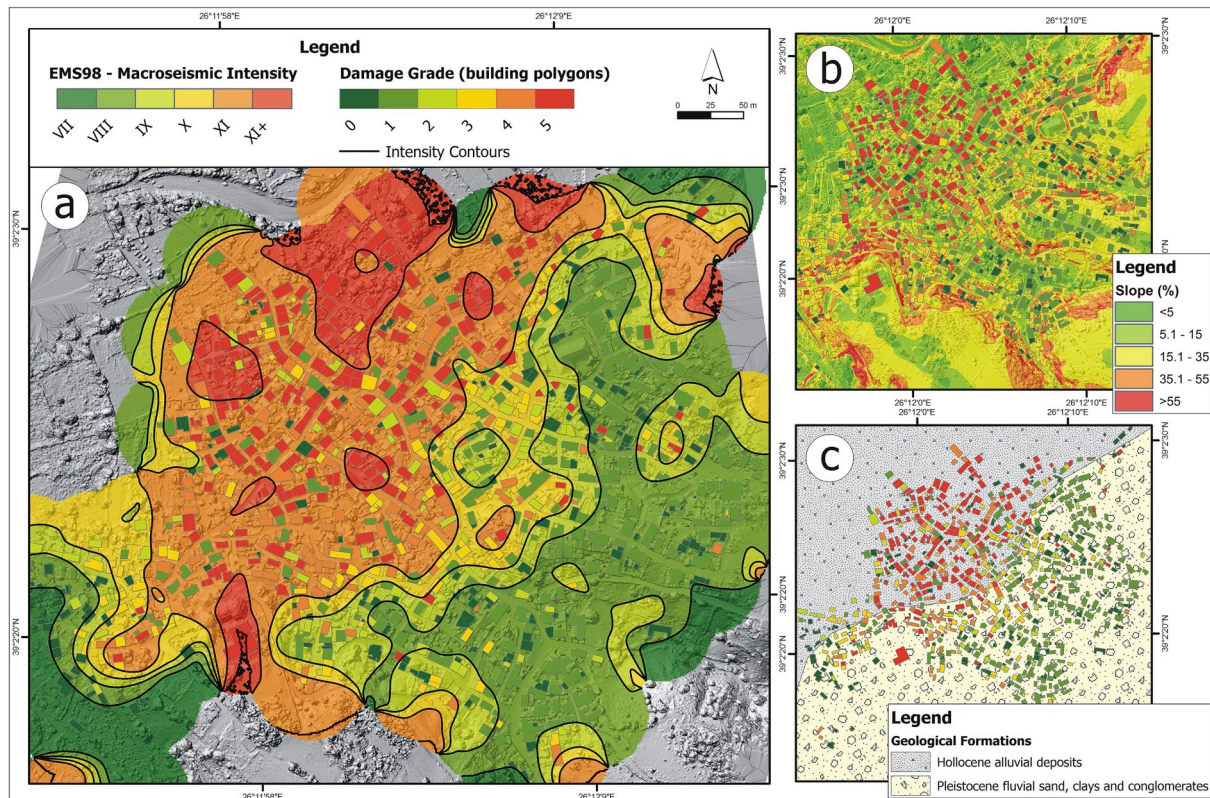


Fig. 17. (a) Isoseismal map for Vrissa settlement after the June 12, 2017 Mw 6.3 Lesvos earthquake based on the application of the EMS-98. (b) Geological map of the broader area of Vrissa. (c) Slope map of Vrissa (values %).

survey and processing for the highest possible detail. Moreover, the EMS-98 was applied comprising differentiation and classification of structures into dominant building types and then into vulnerability classes as well as the classification of building damage into damage grades. Based on the results derived from the application of the EMS-98, a methodology for isoseismal maps drawing was developed and an isoseismal map for the 2017 Lesvos earthquake most affected area was presented.

The presented methodology comprised the following steps, which are also summarized in Fig. 18:

- Building-by-building inspection using GIS desktop and online applications
- UAV post-earthquake disaster survey in the field comprising the deployment of an Unmanned Aircraft System. The survey took place shortly after the earthquake, so that the disaster scene was almost intact by cleaning and demolition works. The flight plan was designed to cover the whole area of the settlement. Pix4D capture was used to create a suitable 3D map flight plan, taking images along two perpendicular directions. Two consecutive flights were executed to collect imagery and 439 images were taken.
- Process of images in the Pix4D mapper software. In the first phase of modeling, the 3D model of the settlement was produced, along with the orthophotomosaic and Digital Surface Model and Digital Terrain Model of the earthquake-affected area.
- The Digital Surface Model was introduced to ESRI ArcMap and through raster filtering of differences between DSM and DTM, building polygons were obtained.
- Through the combination of field observations and onscreen investigation building by building, vulnerability classes and damage grades were assigned to each building polygon.
- A vulnerability class map and a damage grade map were produced with the building polygons.
- Polygons were processed to produce centroid points for every building, bearing the building attributes, in order to enable spatial calculations.
- Point density (N), weighted point density (D), Kernel density and weighted Kernel density maps were constructed through neighborhood analysis of damage grades of centroids.
- Raster calculation between N and D maps (N/D) provided the final maps of damage grade distribution.
- Neighborhood statistics were matched to EMS intensity values, and N/D maps were matched to intensity values.
- An isoseismal map for the earthquake most affected area is the final product. The presented methodology of isoseismal map drawing is another important element for the complete and accurate assessment of the earthquake impact on the affected area and the drawing of important conclusions about the factors controlling damage distribution and for the future mitigation of the disastrous consequences of a similar event.

Based on the results of the field reconnaissance in the devastated settlement of Vrissa, it is concluded that residential buildings with masonry load-bearing walls comprise the majority of the building stock. Based on the EMS-98, they classified mainly as vulnerability class C and they suffered mostly damage grade 5 and 4 (47.2% and 18.1% of the total buildings of Vrissa).

Special structures including temples, post-byzantine structures, museums, schools and industrial buildings with masonry load-bearing walls suffered similar damage with the masonry residential buildings. All R/C buildings constructed during the last decades showed good performance during the 2017 Lesvos earthquake since none of them suffered heavy structural damage.

The western part of Vrissa along with isolated areas of its southern part suffered damage that corresponds to $XI_{+EMS-98}$ intensity. Taking into account the methodology applied for the EMS-98 seismic

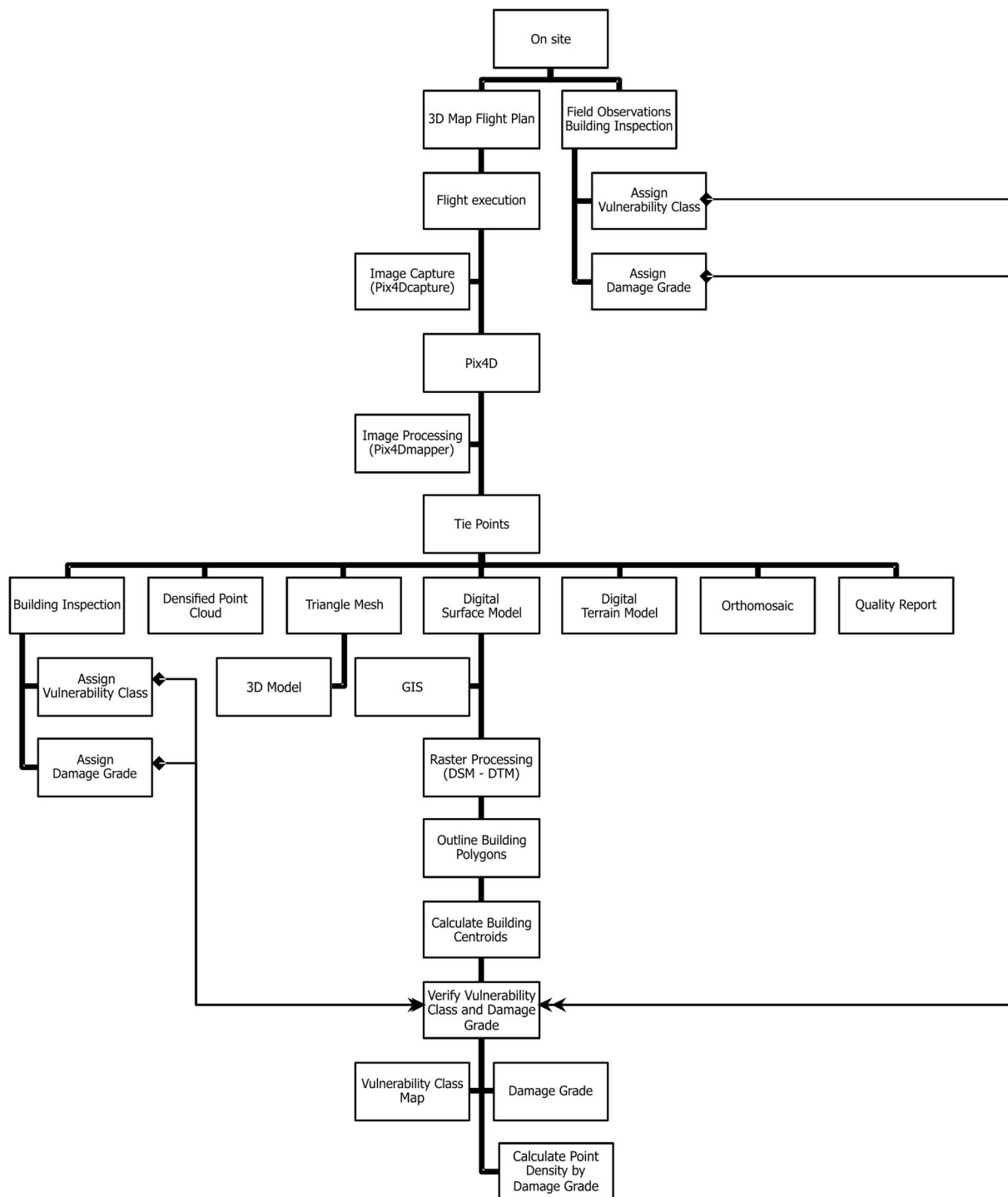


Fig. 18. Overall methodology work flow from field work to the development of the isoseismal map.

intensities assignment in Vrissa settlement, the following remarks can be made:

- Damage assessment was only applicable for C Class buildings, due to their overwhelming majority in the settlement (> 99%).
- Most of buildings with damage grade 5 were located within the area of low slope angles and low elevation, with the exception of the southwestern part of the village.
- Raw damage distribution shows a linear development of maximum damage for the northwestern part of the village. However, this shape is biased by the building distribution and density of the village.
- Weighted damage distribution shows a NNE-SSW zone of maximum damage, equivalent to XI + EMS-98 intensity.
- Intensity XII_{EMS-98} was not applied, due to lack of adequate number of RC buildings to certify it, although there are areas where all buildings of vulnerability class C collapsed.
- The very heavy structural damage was observed in the western part of Vrissa, while its eastern part remained relatively intact. This damage scene is attributed to the synergy of the near-field location of Vrissa, recent deposits, geotechnically unstable zones, proximity to active faults, rupture directivity phenomena and vulnerable buildings.

From the aforementioned, it is concluded that the present study is a complete and comprehensive approach for the earthquake-induced damage assessment from the first step of the building-by-building inspection supported and enhanced by means of desktop and web GIS applications and UAV survey for mapping of the damage scene to the last step of drawing conclusions for the factors affecting and controlling damage type and distribution. Moreover, this study highlights the integration of typical damage assessment methods with modern and innovative techniques adjusted to the field macroseismic survey needs as it comprises building-by-building inspection, use of GIS applications, UAV survey (in-flight) and digital post processing (post-flight), extraction of data and information related to the buildings of the affected area, application of the EMS-98 and assignment of macroseismic intensities and finally correlation of all the aforementioned data with the geological, geomorphological, geotechnical and seismological properties of the earthquake most affected area along with the characteristics and properties of buildings in the affected area.

Same or similar scientific approach has not been implemented yet. The majority of the related earthquake-induced damage assessment studies refer to separate and autonomous applications comprising either GIS or UAV surveys (e.g. Refs. [14,69–72]). Moreover, the proposed methodologies are applied to small built-up areas such as squares, few structures including residential buildings and historical monuments and infrastructures comprising bridges and roads [13,71–73]. On the other hand, few research teams have applied only UAV methodologies to larger built-up areas comprising small villages [12,14].

Most of these studies aim to test, analyze and validate some best practices for rapid and low-cost documentation of the damage state after the disaster occurrence and the response phase. In contrast, the present methodology was applied from the first hours of the response phase after a strong earthquake with significant impact on the natural and built environment taking into account the characteristics and the conditions of the disaster incident and moreover the fact that the agencies competent to the disaster management and recovery did not have a complete picture of the disaster scene. By applying this approach, all people involved in the disaster response and the civil protection can have a clear, precise and accurate picture of the earthquake impact not only in the worst affected area but also in other areas with building damage and earthquake environmental effects, which is the most significant element for timely and right decisions making.

The UAV survey and the digital post processing gave the possibility to verify the field observations throughout the affected area and to apply the EMS-98 with modern and innovative techniques and assign macroseismic intensities by using not only field but also aerial observations.

The post-disaster mapping and damage assessment in general and post-earthquake damage assessment in particular have a lot to gain from the use of modern and innovative techniques such as the use of UAV and GIS based technologies. In comparison with the traditional remote sensing data, the data acquired from UAV aerial survey (in-flight) and the products derived from digital post processing (post-flight) are still much more detailed and accurate revealing a precise image of the affected areas (e.g. [8]). Higher spatial resolution with rich and clear spatial details and higher overlapping are the most significant advantages of UAV images compared with satellite imagery.

This precision and accuracy is very important not only for the effective disaster response but also for the subsequent management and recovery phase. All agencies competent in disaster response, management and recovery can benefit from this critical information rapidly collected by the use of UAV and directly distributed by the use of online GIS applications and platforms. The degree of benefit always depends on the characteristics and the conditions of the disaster incidents.

The integration of UAV and web GIS applications during a rapid post-earthquake field macroseismic reconnaissance can potentially be considered as a methodological framework that can be applied for similar analysis in other areas affected not only by earthquake disasters

but also by other extreme geological, hydrological and meteorological events that have the potential to cause destructive effects on the natural environment, humans and infrastructures.

Appendix A. Supplementary data

Supplementary data to this article can be found online at <https://doi.org/10.1016/j.ijdr.2019.101169>.

References

- [1] F. Dell'Acqua, P. Gamba, Remote sensing and earthquake damage assessment: experiences, limits, and perspectives, *Proc. IEEE* 100 (10) (2012) 2876–2890 <http://doi.org/10.1109/JPROC.2012.2196404>.
- [2] M. Erdik, K. Sesetyan, M.B. Demircioglu, C. Zulfikar, U. Hancilar, C. Tuzun, E. Harmandar, Rapid earthquake loss assessment after damaging earthquakes, in: A. Ansal (Ed.), *Perspectives on European Earthquake Engineering and Seismology, Geotechnical, Geological and Earthquake Engineering*, vol. 34, 2014, pp. 53–96 (1), <http://doi.org/10.1007/978-3-319-07118-3>.
- [3] J. Fernandez Galarreta, N. Kerle, M. Gerke, UAV-based urban structural damage assessment using object-based image analysis and semantic reasoning, *Nat. Hazards Earth Syst. Sci.* 15 (6) (2015) 1087–1101 <http://doi.org/10.5194/nhess-15-1087-2015>.
- [4] S. Ghosh, B.J. Adams, J.A. Womble, C. Friedland, R.T. Eguchi, Deployment of remote sensing technology for multi-hazard post-katrina damage assessment, 2nd International Conference on Urban Disaster Reduction, Taipei, November 27–29, National Science and Technology Center for Disaster Reduction (NCDR), Taiwan, Institute of Social Safety Sciences (ISSS), Japan; and Earthquake Engineering Research Institute (EERI), United States, 2007 8p.
- [5] A. Lessard-Fontaine, F. Alschner, D. Soesilo, Drones in Humanitarian Action - Case Study No. 6: Rapid Damage Assessments of Tabarre and Surrounding Communities in Haiti Following Hurricane Sandy, Geneva, Switzerland (2016) <https://goo.gl/sTUId5> (accessed 2016).
- [6] S. Mavroulis, E. Lekkas, P. Carydis, Using Unmanned Aerial Vehicles for Post-Earthquake Field Reconnaissance: the 2016 August 24 Mw 6.2 Amatrice (Central Italy) Earthquake, *Safe Athens 2017 - New Technologies at the Service of Civil Protection*, Book of Abstracts, 2017, p. 67 <http://safeathens.gr/files/Safe%20Athens%20program-final.pdf>.
- [7] OCHA Policy Development and Studies Branch, Unmanned Aerial Vehicles in Humanitarian Response, (2014) <http://www.unocha.org/sites/unocha/files/Unmanned%20Aerial%20Vehicles%20in%20Humanitarian%20Response%20OCHA%20July%202014.pdf> (accessed 2014).
- [8] Z. Xu, J. Yang, C. Peng, Y. Wu, X. Jiang, R. Li, Y. Zheng, Y. Gao, S. Liu, B. Tian, Development of an UAS for post-earthquake disaster surveying and its application in Ms7.0 lushan earthquake, Sichuan, China, *Comput. Geosci.* 68 (2014) 22–30 <https://doi.org/10.1016/j.cageo.2014.04.001>.
- [9] V. Baiocchi, D. Dominici, M. Mormile, Unmanned aerial vehicle for post seismic and other hazard scenarios, *WIT Trans. Built Environ.* 134 (2013) 113–122, <https://doi.org/10.2495/SAFE130111>.
- [10] V. Baiocchi, D. Dominici, M. Mormile, UAV application in post-seismic environment, *Proceedings: International Archives of the Photogrammetry, Remote Sensing and Spatial Information Sciences, XI-1/W2, 2013 UAV-g2013, 4-6 September 2013, Rostock, Germany, 2013*.
- [11] F. Yamazaki, T. Matsuda, S. Denda, W. Liu, Construction of 3D models of buildings damaged by earthquakes using UAV aerial images, 10th Pacific Conference on Earthquake Engineering Building an Earthquake-Resilient Pacific, November 2015, pp. 6–8 Sydney, Australia.
- [12] A. Calantropio, F. Chiabrandio, G. Sammartano, A. Spanò, L. Teppati Losè, UAV strategies validation and remote sensing data for damage assessment in post-disaster scenarios, *Int. Arch. Photogramm. Remote Sens. Spat. Inf. Sci. XLII-3/W4* (2018) 121–128 <https://doi.org/10.5194/isprs-archives-XLII-3-W4-121-2018>.
- [13] D. Dominici, M. Alicandro, V. Massimi, UAV photogrammetry in the post-earthquake scenario: case studies in L'Aquila, *Geomatics, Nat. Hazards Risk* 8 (1) (2017) 87–103 <https://doi.org/10.1080/19475705.2016.1176605>.
- [14] S. Li, H. Tang, Building damage extraction triggered by earthquake using the UAV imagery, *The International Archives of the Photogrammetry, Remote Sensing and Spatial Information Sciences, XLII-3 2018*, pp. 929–936 <https://doi.org/10.5194/isprs-archives-XLII-3-929-2018>.
- [15] J. Fernandez Galarreta, Urban Structural Damage Assessment Using Object-Oriented Analysis and Semantic Reasoning, University of Twente, 2014, <http://doi.org/10.5194/nhess-2-5603-2014>.
- [16] J. Palmer, *The potential use of unmanned aerial vehicles during on-site inspections*, *CTBT: Science and Technology*, 2015.
- [17] L. Dong, J. Shan, A comprehensive review of earthquake-induced building damage detection with remote sensing techniques, *ISPRS J. Photogrammetry Remote Sens.* 84 (2013) 85–99 <http://doi.org/10.1016/j.isprsjprs.2013.06.011>.
- [18] F. Alschner, J. DuPlessis, D. Soesilo, Drones in Humanitarian Action - Case Study No. 9: Using Drone Imagery for Real-Time Information after Typhoon Haiyan in the Philippines, Geneva, Switzerland (2013) <https://drones.fsd.ch/en/case-study-no-9-using-drone-imagery-for-real-time-information-after-typhoon-haiyan-in-the-philippines/>.
- [19] P. Meier, D. Soesilo, Drones in Humanitarian Action - Case Study No. 10: Using Drones for Disaster Damage Assessments in Vanuatu, (2015) Geneva, Switzerland. Retrieved from <https://drones.fsd.ch/en/case-study-no-10-monitoring-and-inspection-natural-disaster-i-acute-emergency-i-assessments/>.
- [20] P. Zimmaro, J.P. Stewart, L. Di Sarno, M.G. Durante, A.L. Simonelli, A. Penna,

- Engineering Reconnaissance of the 24 August 2016 Central Italy Earthquake. Version 2, (2016) <http://doi.org/10.18118/G61S3Z>.
- [21] M.W. Smith, J.L. Carrivick, J. Hooke, M.J. Kirkby, Reconstructing flash flood magnitudes using "Structure-from-Motion": a rapid assessment tool, *J. Hydrol.* 519 (PB) (2014) 1914–1927 <http://doi.org/10.1016/j.jhydrol.2014.09.078>.
- [22] E. Andreadakis, M. Diakakis, E. I. Nikolopoulos, N. I. Spyrou, M.E. Gogou, N. K. Katsetsiadou, G. Deligiannakis, A. Georgakopoulos, Z. Antoniadis, M. Melaki, E. Lekkas, J. Kalogiros, Characteristics and impacts of the November 2017 catastrophic flash flood in Mandra, Greece, *Geophysical Research Abstracts*, Vol. vol. 20, EGU2018-12215, EGU General Assembly 2018, Vienna, 8 April, 2018.
- [23] M. Diakakis, E. Andreadakis, E.I. Nikolopoulos, N.I. Spyrou, M.E. Gogou, G. Deligiannakis, N.K. Katsetsiadou, Z. Antoniadis, M. Melaki, A. Georgakopoulos, K. Tsaprouni, J. Kalogiros, E. Lekkas, An integrated approach of ground and aerial observations in flash flood disaster investigations. The case of the 2017 Mandra flash flood in Greece, *Int. J. Disaster Risk Reduct.* (2018), <https://doi.org/10.1016/j.ijdrr.2018.10.015>.
- [24] G. Grünthal, European Macroseismic Scale 1998 EMS-98, Conseil de l'Europe vol. 15, Cahiers du Centre Européen de Géodynamique et de Séismologie, Luxembourg, 1998.
- [25] University of Athens Seismological Laboratory, Significant Earthquakes in Greece during 2017, (2017) http://www.geophysics.geol.uoa.gr/stations/gmaps3/gmapv3_significant.php?mapmode=mech&lng=en&year=2017 (accessed 2017).
- [26] N. Ambrasey, Earthquakes in the Mediterranean and Middle East: a Multidisciplinary Study of Seismicity up to 1900, Cambridge University Press, 2009.
- [27] B.C. Papazachos, C.B. Papazachou, *The Earthquakes of Greece*, Zitis, Athens, 1989.
- [28] B.C. Papazachos, C.B. Papazachou, *The Earthquakes of Greece*, Zitis, Athens, 1997.
- [29] B.C. Papazachos, C.B. Papazachou, *The Earthquakes of Greece*, Zitis, Athens, 2003.
- [30] K. Taxeidis, Study of Historical Seismicity of the Eastern Aegean Islands, PhD thesis National and Kapodistrian University of Athens, Greece, 2003, p. 301 <http://macroseismology.geol.uoa.gr/studies/TAXE003.pdf>.
- [31] J. Hecht, Geological Map of Greece, Plomari-Mytlini Sheet vol. 1, Institute of Geology and Mineral Exploration of Greece scale, 1972 50,000.
- [32] J. Hecht, Geological Map of Greece (1:50,000), Methymna Sheet, IGME, 1974.
- [33] J. Hecht, Geological Map of Greece (1:50,000), Eressos Sheet, IGME, 1974.
- [34] J. Hecht, Geological Map of Greece (1:50,000), Polichnitos Sheet, IGME, 1974.
- [35] G. Katsikatsos, D. Mataragas, G. Migiros, E. Triandafyllou, Geological Study of Lesbos Island, IGME, 1982.
- [36] G. Pe-Piper, Cainozoic Volcanic Rocks of Lesbos Island, Ph.D. Thesis University of Patras, 1978, pp. 1–365.
- [37] G. Pe-Piper, D.J.W. Piper, Revised stratigraphy of the Miocene volcanic rocks of Lesbos, Greece, *Neues Jahrbuch Geol. Palaontol. Monatsh.* 2 (1993) 97–110.
- [38] A. Chatzipetros, A. Kiratzi, S. Sboras, N. Zouros, S. Pavlides, Active faulting in the North-eastern Aegean Sea islands, *Tectonophysics* 597–598 (2013) 106–122.
- [39] J. Mascle, L. Martin, Shallow structure recent evolution of the Aegean Sea: a synthesis based on continuous reflection profiles, *Mar. Geol.* 94 (1990) 271–299 [https://doi.org/10.1016/0025-3227\(90\)90060-W](https://doi.org/10.1016/0025-3227(90)90060-W).
- [40] K. Makropoulos, G. Kaviris, V. Kouskouna, An updated and extended earthquake catalogue for Greece and adjacent areas since 1900, *Nat. Hazards Earth Syst. Sci.* 12 (2012) 1425–1430 <https://doi.org/10.5194/nhess-12-1425-2012>.
- [41] M. Stucchi, A. Rovida, A.A. Gomez Capera, P. Alexandre, T. Camelbeeck, M.B. Demircioglu, P. Gasperini, V. Kouskouna, R.M.W. Musson, M. Radulian, K. Sesetyan, S. Vilanova, D. Baumont, H. Bungum, D. Fäh, W. Lenhardt, K. Makropoulos, J.M. Martinez Solares, O. Scotti, M. Zivcic, P. Albini, J. Batlo, C. Papaioannou, R. Tatevossian, M. Locati, C. Meletti, D. Viganò, D. Giardini, The SHARE european earthquake catalog (SHEEC) 1000–1899, *J. Seismol.* 17 (2) (2013) 523–544.
- [42] N. Voulgaris, I. Parcharidis, M. Pahoul, E. Pirlis, Correlation of tectonics, seismicity and geothermics of Lesbos Island using remote sensing data and Geographical Information Systems, *Bull. Geol. Soc. Greece XXXVI* (2004) 938–947.
- [43] E. Lekkas E, Macroseismicity and geological effects of the Wenchuan earthquake (ms 8.0r - 12 May 2008), Sichuan, China: macro-distribution and comparison of EMS1998 and ESI2007 intensities, *Bull. Geol. Soc. Greece* 43 (2010) 1361–1372.
- [44] E. Lekkas, The 12 May 2008 Mw 7.9 Wenchuan, China, earthquake: macroseismic intensity assessment using the EMS-98 and ESI 2007 scales and their correlation with the geological structure, *Bull. Seismol. Soc. Am.* 100 (2010) 2791–2804, <https://doi.org/10.1785/0120090244> 5B.
- [45] N.D. Delibasis, N.S. Voulgaris, Microseismic and seismotectonic study of the island of Lesbos, *Proc. Fourth Inter. Sem. Res. EC Geothermal Energy Res. And Demo.*, Florence, 27–30 April 1989, Kluwer Academic Publishers, 1989, pp. 474–481.
- [46] G.A. Papadopoulos, A. Agalos, M. Charalampakis, T. Novikova, I. Triantafyllou, A. Yalciner, The Lesbos Isl. strong (Mw6.3) earthquake of 12 June 2017, its rupture process and the associated small tsunamis, *Safe Athens 2017, New Technologies at the Civil Protection Service*, 28–30 June 2017, Athens, Greece, 2017.
- [47] P. Papadimitriou, I. Kassaras, G. Kaviris, G.A. Tselentis, N. Voulgaris, E. Lekkas, G. Chouliaras, C. Evangelidis, K. Pavlou, V. Kapetanidis, A. Karakonstantis, D. Kozantzidou-Firtinidou, I. Fountoulakis, C. Millas, I. Spingos, T. Aspiotis, A. Mounoulidou, E. Skourtsos, V. Antoniou, E. Andreadakis, S. Mavroulis, M. Kleanthi, The 12th June 2017 Mw = 6.3 Lesbos earthquake from detailed seismological observations, *J. Geodyn.* 115 (2018) 23–42 <https://doi.org/10.1016/j.jog.2018.01.009>.
- [48] E. Lekkas, N. Voulgaris, P. Carydis, E. Skourtsos, E. Andreadakis, S. Mavroulis, V. Antoniou, P. Papadimitriou, G.A. Tselentis, V. Kouskouna, G. Kassaras, G. Kaviris, K. Pavlou, V. Sakkas, The Lesbos earthquake (North Aegean, Mw 6.3, 12/06/2017): preliminary scientific results and emergency management, *Proceedings: Safe Athens 2017, New Technologies at the Civil Protection Service*, 28–30 June 2017, Athens, Greece, 2017.
- [49] Natural Disaster Rehabilitation Directorate, Results from the First Building Inspection from June 13th to June 24th 2017, (2017) <http://www.yas.gr> (accessed 2017).
- [50] D. DiBiase, A.M. MacEachren, J.B. Krygier, C. Reeves, Animation and the role of map design in scientific visualization, *Cartogr. Geogr. Inf. Syst.* 19 (2) (1992) 201–214.
- [51] G. Newman, D. Zimmerman, A. Crall, M. Laituri, J. Graham, L. Stapel, User-friendly web mapping: lessons from a citizen science website, *Int. J. Geogr. Inf. Sci.* 24 (12) (2010) 1851–1869.
- [52] E. Lekkas, The Athens earthquake (7 September 1999): intensity distribution and controlling factors, *Eng. Geol.* 59 (2001) 297–311.
- [53] A. Tertulliani, L. Arcoraci, M. Berardi, F. Bernardini, R. Camassi, R. C. Castellano, S. Del Mese, E. Ercolani, L. Graziani, I. Leschiutta, A. Rossi, M. Vecchi, An application of EMS98 in a medium-sized city: the case of L'Aquila (Central Italy) after the April 6, 2009 Mw 6.3 earthquake, *Bull. Earthquake* 9 (2011) 67–80.
- [54] S.D. Mavroulis, I.G. Fountoulis, E.N. Skourtsos, E.L. Lekkas, I.D. Papanikolaou, Seismic intensity assignments for the 2008 Andravida (NW Peloponnese, Greece) strike-slip event (June 8, Mw=6.4) based on the application of the Environmental Seismic Intensity scale (ESI 2007) and the European Macroseismic scale (EMS-98), Geological structure, active tectonics, earthquake environmental effects and damage pattern, *Ann. Geophys.* 56 (2013) S0681 <https://doi.org/10.4401/ag-6239>.
- [55] I.G. Fountoulis, S.D. Mavroulis, Application of the environmental seismic intensity scale (ESI 2007) and the European macroseismic scale (EMS-98) to the Kalamata (SW Peloponnese, Greece) earthquake (Ms=6.2, September 13, 1986) and correlation with neotectonic structures and active faults, *Ann. Geophys.* 56 (2013) S0675 <https://doi.org/10.4401/ag-6237>.
- [56] S. Mavroulis, V. Alexoudi, A. Grambas, E. Lekkas, P. Carydis, The January-February 2014 Cephalonia (Ionian Sea, western Greece) earthquake sequence: damage pattern on buildings, 16th World Conference of Earthquake Engineering, Santiago, Chile, 2017, p. 12 (In: 96 Special Session - Evolution of EMS-98 Building Types, Vulnerability Classes and Damage Grade Description towards an International Macroseismic Scale), Paper No 414.
- [57] P. Carydis, E. Lekkas, Th. Kritikos, The Mw 7.1 Sept 4 2010 and Mw 6.3 Febr 22 2011, New Zealand eqs. Comparison of EMS1998 and ESI2007 data, 15th World Conference on Earthquake Engineering (15WCEE), 2012 Paper No. 0190, Lisbon, 2012.
- [58] S.T. Maqsood, J. Schwarz, M. Edward, Application of the European macroseismic scale – 1998 in the Asia-Pacific region, in: C. Adam, R. Heuer, W. Lenhardt, C. Schranz (Eds.), *Vienna Congress on Recent Advances in Earthquake Engineering and Structural Dynamics 2013 (VEESD 2013)*, 2013 28–30 August 2013, Vienna, Austria Paper No. 470.
- [59] S.M. McGowan, K.S. Jaiswal, D.J. Wald, Using structural damage statistics to derive macroseismic intensity within the Kathmandu valley for the 2015 M7.8 Gorkha, Nepal earthquake, *Tectonophysics* (2016) 158–172 <https://doi.org/10.1016/j.tecto.2016.08.002>.
- [60] J. Schwarz, L. Abrahamczyk, M. Leipold, T. Wenk, Vulnerability assessment and damage description for R.C. frame structures following the EMS-98 principles, *Bull. Earthq. Eng.* 13 (2015) 1141–1159 <https://doi.org/10.1007/s10518-014-9694-x>.
- [61] R. Koldewey, *Die antiken Baureste der Insel Lesbos*, Berlin, 1890.
- [62] Theodoulou, Ephorate of marine antiquities: underwater research at the ancient harbours of Lesbos, *Archaeology* 116 (2010) 93–102.
- [63] K.A. Tselekas, My Village: Vrissa of Lesbos, Aeolida, Thessaloniki, 2010, p. 382.
- [64] N. Karydis, Traditional antiseismic structure in the eastern Aegean: the case of Eressos and pergamon, *Proceedings: 3rd Panhellenic Conference on Earthquake Engineering & Seismology*, 5–7 November 2008, 2008.
- [65] N. Karydis, Eressos: the House, the Construction, the Settlement, Papatotiriou publications, 2003.
- [66] Earthquake Planning and Protection Organization, Greek Antiseismic Code 2000-EAK, Ministry of Environment, Planning and Public Works, Athens, 2000.
- [67] B. Silverman, *Density Estimation for Statistics and Data Analysis*, Chapman and Hall, London, 1986.
- [68] A. Kiratzi, The 12 June 2017 Mw 6.3 Lesbos Island (Aegean Sea) earthquake: slip model and directivity estimated with finite-fault inversion, *Tectonophysics* (2018), <https://doi.org/10.1016/j.tecto.2018.01.003>.
- [69] D. Dominici, M. Alicandro, V. Massimi, UAV photogrammetry in the post-earthquake scenario: case studies in L' Aquila, *Geomatics, Nat. Hazards Risk* 8 (1) (2017) 87–103 <https://doi.org/10.1080/19475705.2016.1176605>.
- [70] D. Duarte, F. Nex, N. Kerle, G. Vosselman, Towards a more efficient detection of earthquake induced façade damages using oblique UAV imagery, *The International Archives of the Photogrammetry, Remote Sensing and Spatial Information Sciences*, XLII-2/W6, 2017, pp. 93–100 <https://doi.org/10.5194/isprs-archives-XLII-2-W6-93-2017>.
- [71] F. Yamazaki, K. Kubo, R. Tanabe, W. Liu, Damage assessment and 3D modelling by UAV flights after the 2016 Kumamoto, Japan earthquake, 2017 IEEE International Geoscience and Remote Sensing Symposium, July 23–28, 2017, Fort Worth, Texas, USA, 2017.
- [72] F. Yamazaki, T. Matsuda, S. Denda, W. Liu, Construction of 3D models of buildings damaged by earthquakes using UAV aerial images, *Proceedings of the Tenth Pacific Conference on Earthquake Engineering Building an Earthquake-Resilient Pacific* 6–8 November 2015, Sydney, Australia, 2015, pp. 204–212.
- [73] F. Yamazaki, W. Liu, Remote sensing technologies for post-earthquake damage assessment: a case study on the 2016 Kumamoto earthquake, 6th ASIA Conference on Earthquake Engineering (6ACEE) 22–24 Sept 2016, Cebu City, Philippines, 2016.